THE ROLE OF WATER SOLUBILITY AND DIFFUSION COEFFICIENT IN AIR OF CHLORINE DIOXIDE GAS DURING SURFACE DECONTAMINATION AND COMPATIBILITY OF SELECTED PLASTICS AND ELASTOMERS

A Thesis Presented for the
Master of Science
Degree
The University of Tennessee, Knoxville

Mario Ernesto Bermudez Gonzalez
December 2020

DEDICATION

This study is wholehearted to my family, especially my beloved parents (Nelly & Douglas) and sister (Marthanelly), who have been my source of inspiration, and continually provide me their moral, emotional support.

To my beloved partner (Tania), who despite the distance encouraged me and gave me strength and love when I thought of giving up.

Finally, yet importantly, I dedicate this work to the Almighty God.

ACKNOWLEDGEMENTS

I would like to express my gratitude to my advisor, Dr. Mark Morgan, for his mentorship during my MS program at the Food Science department. Thank you for teaching me to think critically and independently, for giving me the opportunity to fulfill my program, and meet so many wonderful people during this journey.

I am also grateful for the presence of my committee members Dr. Jiajia Chen, and Dr. Tao Wu. Thank you for your valuable input and discussion, and for being a substantial part of this study. Also, to Dr. William Hart, who share his expertise with me, and Dr. Xiaocun Sun for her support during the data analysis.

Finally, I would like to thank my friends, #LatinoGang, colleagues, graduate students, and faculty & staff in the Food Science Department for their time and advice, which helped me get through.

ABSTRACT

Food safety is a concern for all individuals involved in the food supply chain. Besides controlling the food product itself to improve safety, washing and sanitizing surfaces and equipment are critical. Chlorine dioxide (ClO_2) is a green-yellow gas, known as a strong antimicrobial agent against multiple pathogenic microorganisms and effective on biofilms. Plastics such as polypropylene (PP), polyester (PET), cast nylon, ultra-high-molecular-weight polyethylene (UHMWPE), polytetrafluoroethylene (PTFE), polyvinylidene fluoride (PVDF) and white Acetal; and elastomers like nitrile rubber (Buna-N), ethylene propylene diene monomer (EPDM), and fluoroelastomer (FKM) are widely used in food processing surfaces and equipment. However, few studies have been conducted to address the interaction of gas with materials that might be present during the decontamination procedure nor the change in mechanical properties of plastics and elastomers. The objectives of this study were to measure ClO_2 gas interaction with water, simulate transport into stainless steel crevices during surface decontamination, and determine the resistance to ClO_2 gas for selected materials. The gas was circulated inside a closed chamber with three different volumes of deionized water (20, 40, and 60 mL), and 0 mL (control). The gas decay was monitored and recorded until the concentration dropped below the detection limit. A physics-based simulation model was developed using COMSOL and validated by previously reported results in the literature, and additional data obtained during this experiment. A mathematical model was proposed for analyzing the time needed for ClO_2 gas to reach the bottom of any possible crevice during equipment surface decontamination, which is depth-dependent. Additionally, selected materials were exposed to 3000 ppm [parts per million] for 7 days inside a chamber following ASTM International Standards. Results showed an increase in the reaction rate due to water presence at different water volume and exposure surface area. After 7 days' exposure at 3000 ppm of ClO2 gas, none of the selected plastics or elastomers showed a significance difference ($p<0.05$) in the hardness value. This can help the food processing industry in constructing an effective gas sanitation system and establishing optimum sanitizing treatment conditions.

TABLE OF CONTENTS

CHAPTER I Literature review 1
1.1. Food safety 1
1.1.1. Foodborne pathogens in food processing 3
1.1.2. Decreasing foodborne illness through sanitation 4
1.2. Chlorine dioxide 6
1.2.1. Antimicrobial activity 7
1.2.2. Photochemical dissociation 10
1.2.3. Solubility in water 17
1.2.4. Diffusion coefficient properties 19
1.2.5. Analytical method to measure concentration 21
CHAPTER II Role of water solubility and diffusion in modeling the gas transport involved in surface decontamination with chlorine dioxide gas 23
2.1. Abstract 24
2.2. Introduction 25
2.3. Materials and methods 27
2.3.1. Schematic system - exposure chamber 27
2.3.2. Chlorine dioxide gas concentration decay over time 29
2.3.3. Simulation model development: Geometric model 30
2.3.4. Simulation model development: Governing equations 30
2.3.5. Simulation model development: Model validation 31
2.3.6. Simulation model development: Simulation model of ClO_2 gas diffusion in air into crevices 33
2.3.7. Statistical analysis 33
2.4. Results and discussion 33
2.4.1. Chlorine dioxide gas concentration decay over time 33
2.4.2. Simulation model validation 41
2.4.3. Simulation model ClO_2 gas diffusion in the air into crevices 44
2.4.4. Simulation model ClO_2 gas diffusion in the air into crevices with water present 46
2.5. Conclusions 47
CHAPTER III Chlorine dioxide gas compatibility of plastics and elastomers typically used in food processing equipment 52
3.1. Abstract 53
3.2. Introduction 53
3.3. Materials and methods 55
3.3.1. Schematic system - gas generation 55
3.3.2. Material Samples 56
3.2.3. Exposure Tests 57
3.3.4. Hardness measurement 57
3.3.5. Color measurement 60
3.3.6. Statistical analysis of data 60
3.4. Results and discussion 61

3.4.1. Hardness measurement.....61
3.4.1. Hardness measurement.....62
3.4.2. Color measurement 62
3.5. Conclusions.....68
List of References.....69
VITA.....74

LIST OF TABLES

Table 1. Summary of research studies on antimicrobial efficiencies of chlorine dioxide for food products 11
Table 2. Experimental parameters for the chlorine dioxide gas diffusion used in the model 34
Table 3. First-order reaction rate k_1 [1/h] of ClO_2 gas at different volume of deionized water and different exposure surface area 39
Table 4. First-order reaction rate k_2 [1/h] of ClO_2 gas at different volume of deionized water and different exposure surface area. 40
Table 5. Average concentration (mg/L) at the bottom of the crevice over time. Using a diffusion coefficient of 0.145 cm^2/s 48
Table 6. Average concentration (mg/L) at the bottom of the crevice over time. Using a diffusion coefficient of 0.097 cm^2/s 49
Table 7. Average concentration (mg/L) at the bottom of the crevice over time with water presence in the wall surface. Using a diffusion coefficient of 0.145 cm^2/s 50
Table 8. Average concentration (mg/L) at the bottom of the crevice over time with water presence in the wall surface. Using a diffusion coefficient of 0.097 cm^2/s 51
Table 9. Durometer equipment amount of compressive force [N] 60
Table 10. Material dimensions 61
Table 11. Mechanical properties value for seven different plastics exposed to ClO2 gas (3000 ± 100 ppm) for 0, and 7 days 64
Table 12. Mechanical properties value for three different elastomers exposed to ClO2 gas (3000 ± 100 ppm) for 0, and 7 days 64
Table 13. Color properties of selected plastics and elastomers exposed for 0, 7, 14, and days to ClO_2 gas (3000 ppm) Material exposed for 14 and 21 days was not replicated 66

LIST OF FIGURES

Figure 1. The effect of pH on aqueous solution of chlorine and chlorine dioxide at different concentration required to kill 99% of solutions containing 15,000 viable cells of *E. coli* at pH of 6.5 and 8.5. Adapted from (Gates, 1998).....8
Figure 2. Mechanism of action of Chlorine Dioxide against pathogenic microorganisms. Adapted from (Sun, Baldwin, & Bai, 2019) 9
Figure 3. OClO absorption spectrum. Upper figure: OClO absorbance' peaks. Lower figure: OClO vibrational near to 400 nm. Adapted from (Davis & Lee, 1996). 17
Figure 4. Schematic representation of the photo reactivity of OCIO in gas-phase. Adapted from (Vaida & Simon, 1995). 18
Figure 5. Schematic set up for chlorine dioxide depletion by deionized water. Dashed area shows the closed system that was monitored as gas concentration decayed over time. 28
Figure 6. Chlorine dioxide gas diffusion from a reservoir to a collector through a diffusion tube. Adapted from (Lee, Burgess, Rubino, & Auras, 2015).....31
Figure 7. Chlorine dioxide concentration versus time for control and different volume of deionized water at surface area of 1.819×10^{-3} m^2. Values fitted of first-order reaction equations 2.3.2 (for control) and 2.3.4 for 20, 40 and 60 ml. 35
Figure 8. Raw data fitted to the two-term exponential decay of ClO_2 gas concentration over time for varying water volumes at a constant surface areaa of 2.16, 18.19, and 64.18 cm^2.....36
Figure 9. Meshing scheme of the diffusion tube and collector vessel. 41
Figure 10. Comparison between predicted values (Equation 2.3.8 & COMSOL simulation) and observed values of ClO_2 concentration (mg/L) at the collector vessel during diffusion through 4.76 mm x 100mm tube with different diffusion coefficients.....43
Figure 11. Comparison between predicted values (Equation 2.3.8 & COMSOL simulation) and observed values of ClO_2 concentration (mg/L) at the collector vessel during diffusion through 4.76 mm x 100mm tube 44
Figure 12. Schematic setup for evaluating material compatibility to constants ClO_2 gas exposure.....58
Figure 13. Schematic description of durometer equipment. Adapted from ASTM International Standard D2240-15.....59
Figure 14. Plastics Young's module [MPa] value after ClO_2 gas exposure for 7 days at 3000 ppm. 63
Figure 15. Elastomers hardness (N) value after and before ClO_2 gas exposure for 7 days at 3000 ppm 63

CHAPTER I
LITERATURE REVIEW

1.1. Food safety

Foodborne disease, also known as foodborne illness or food poisoning, results from the consumption of food contaminated with pathogenic bacteria, viruses, or parasites. The main sources of contamination are mostly unhygienic practices during food production, harvesting, preparation, and equipment cleaning, and the lack of good agricultural practices as well (Adley & Ryan, 2016). The U.S. Centers for Disease Control and Prevention estimates that each year around 9.4 million sicknesses and 2600 deaths occur due to foodborne disease (Scallan, Hoekstra, Angulo, Tauxe, Widdowson, Roy, et al., 2011). Foodborne disease outbreaks caused by microorganisms are one of the major concerns for food processors and marketers due to economic losses and brand reputation (Scallan, et al., 2011). Despite several studies carried out in this field, globally, foodborne illness is not under absolute control, hence new techniques and practices to decrease its incidence are needed.

Several studies reported the negative effect of food recalls directly to that specific industry. Annually, healthcare and losses because of foodborne disease are estimated to $150 billion in the United States (Scharff, 2012). According to Southern Agricultural Economics the *Salmonella* outbreak in ground beef in 2009 decreased purchase of this product by 17 percent in Utah for four weeks after the recall (Zare, Zheng, & Buck, 2017). In 2003 Bovine Spongiform Encephalopathy (BSE) was discovered in the United States. The impact post recall resulted in decreasing consumption of 0.26 pounds per person for the following two weeks, implicating around $97 million in losses to the beef industry over the period (M. Taylor, Klaiber, & Kuchler, 2016).

Food recalls have been a concern in the global food industry because they result in significant losses for food production, processing, and marketing firms. For meat and poultry processors, a Class I recall can promote a reduction in shareholders' wealth equal to approximately $109 million, after five days of the actual recall. These findings might be due to Class I recall and perceived health risks of their products, impacting future income for the firm since profits are affected by consumers' and customers' reactions to health concerns (Pozo & Schroeder, 2016).

Historically, there are 31 pathogens known to cause the majority of foodborne diseases, these include 21 bacteria, five viruses, and five parasites (Adley & Ryan, 2016). According to CDC, the following eight pathogens: *Salmonella, Clostridium perfringes, Campylobacter, Staphylococcus aureus, Escherichia coli* O157:H7,

Listeria monocytogenes, Norovirus and *Toxoplasma gandii* are responsible for most of the cases reported (Wolfram, 2017).
Staphylococcal foodborne disease is one of the most common worldwide, as a result of eating food contaminated by preformed *Staphylococcus aureus* enterotoxins. *S. aureus* is responsible for approximately 241 thousands illness annually. However, the actual incidence might be a lot higher due to a large number of foodborne illnesses that are not reported in the United States (Kadariya, Smith, & Thapaliya, 2014). The bacterium are Gram-positive, non-motile, catalase positive, small, and spherical shaped. The species are distinguished by forming short chains or bunches in grape-like cluster, and can survive a wide temperature range from 7°C to 47.8°C, despite being a mesophile (optimal growth temperature 35°C). The growth pH range is between 4.5 and 9.3 (7.0 – 7.5 optimal pH range).). *S. aureus* is a resistant, non-spore-forming bacteria and can survive for long periods in a dry environment. Several species have the ability to produce heat-stable enterotoxins that cause gastroenteritis (Abraham, Al-Khaldi, Assimon, Beaudry, Benner, Bennett, et al., 2012).

Another microorganism of great interest is *Escherichia coli* (*E. coli*), a Gram negative and rod-shaped bacteria, which can be found in the intestines of people and animals or foods. Most *E. coli* bacteria are harmless and related to a healthy intestinal tract (CDC, 2019; M. Taylor, Klaiber, & Kuchler, 2016). However, there are six acknowledged pathogenic groups, the following four are known to be transmitted throughout contaminated food or water: enterotoxigenic (ETEC), enteropathogenic (EPEC), enterohemorrhagic (EHEC) and enteroinvasive (EIEC). The EHEC group is the one causing most of the foodborne outbreaks around the world. Germany, in 2011, had an outbreak due to *E. coli* strain of serotype O104:H4, which belongs to the EHEC group and produces Shiga toxin, a characteristic of this group (Abraham, et al., 2012).

The first group known to be related to contaminated food or water consumption is the ETEC, characterized due to several virulence factors and heat-labile toxin and heat-stable toxin production. In the United States, consumers' won´t get affected unless they travel to areas with a lack of sanitation procedures, typically in undeveloped countries. This group causes gastroenteritis in humans, so-called traveler´s diarrhea (Abraham, et al., 2012). The second pathogenic group is the EPEC, which involves locus for enterocyte effacement (LEE) pathogenicity island, containing multiple virulence factors causing diarrhea that last for 21 to 120 days. EPEC affects most countries with low or no sanitation, although this illness must be taken seriously because it occurs most often in children under age two (Abraham, et al., 2012).

The third group is the EHEC. As previously mentioned, this group is of great concern for food safety. The *E. coli* bacteria that belong to this group are Shiga toxin producers and cause a spectrum of illnesses such as bloody diarrhea, blood-

clotting problems, kidney failure, and even death. Foodborne outbreaks to this toxin have been associated with ground meats, unpasteurized milk or fruit juice, lettuce, spinach, sprouts, and frozen cookie dough. The serotype O157:H7 is the most common EHEC strain and is responsible for approximately 75% of the infections from this pathogenic group. The symptoms have a duration of typically two to nine days, and a mortality rate of 3% to 5% (Abraham, et al., 2012; Tarr, 1995). The fourth group known as EIEC list a death rate of zero for diarrheagenic. The disease caused by EIEC usually begins as watery diarrhea, then progresses to mild dysentery and might include cramps, vomiting, fever and/or chills (Abraham, et al., 2012).

A serious infection inflicted by contaminated food with *Listeria monocytogenes* is known as Listeriosis, in which 1,600 people (in the US) get sick annually and approximately 260 die. This bacteria is known to infect more pregnant women, which are more susceptible to other people. Despite this, they are more likely to recover their babies usually do not survive. The bacterium is rarely diagnosed as the cause of gastroenteritis and fever, partly because this organism is not detected by routine procedures (Dalton, Austin, Sobel, Hayes, Bibb, Graves, et al., 1997; Scallan, et al., 2011). *L. monocytogenes* is a Gram-positive, rod-shaped, and facultative bacterium, which has a motility by flagella. Despite it not being a leading cause of foodborne outbreaks, this bacterium is one of the leading causes of death from foodborne diseases, with a fatality rate as high as 30%. It can be found in the environment, soil, and decaying vegetation. It is salt tolerant and can survive at conditions below 1°C. Once the consumer is infected, it can cause two types of disease. The first can vary from mild to intense nausea, vomiting, aches, fever, and diarrhea, and generally goes away by itself. However, the second type is more deadly, occurs when the infection spreads to the nervous system resulting as meningitis (Abraham, et al., 2012)

1.1.1. Foodborne pathogens in food processing

In industrial countries, around 30% of the population has sufferred somehow from a foodborne illness. Food contamination may occur due to cross-contamination from ingredients, the processing environment including equipment or surfaces, or people involved in every stage of the process (Barach, Fraser Heaps, Deibel, Mazzotta, Jackson, Scimeca, et al., 2016; WHO, 2002).
Through different steps in the food chain: processing, packaging, transport, and even retail, all wet surfaces that are in direct or indirect contact with food might provide a solid substrate, water and/ or nutrients for the development of organized bacterial ecosystems known as biofilms. Biofilms containing pathogenic microorganisms such as *Bacillus cereus*, *Escherichia coli*, *Shigella* spp., *Staphylococcus aureus, Listeria spp*., *Staphylococcus spp*., and *Vibrio spp* have been detected in dairy, egg, and sea processing industries. (Bridier, Briandet,

Thomas, & Dubois-Brissonnet, 2011; Bridier, Sanchez-Vizuete, Guilbaud, Piard, Naitali, & Briandet, 2015). The bacteria growth on these surfaces is a critical factor that leads to foodborne diseases and has a significant impact on public health.
The development of pathogenic microorganisms in the food processing environment is related to biotic and abiotic factors, where the attachment of cells to processing surfaces may lead to biofilm formation. Most pathogenic microorganism associated to foodborne illness are able to adhere to abiotic surfaces, which can be further subdivided into nonnutritive (plastic, glass, metal, etc.) and nutritive (chitin), and form biofilms on many materials and under almost all the environmental conditions met in varying food facilities (Bridier, Sanchez-Vizuete, Guilbaud, Piard, Naitali, & Briandet, 2015; Davey & O'Toole, 2000). Some researchers have shown the growth and adhesion of pathogenic microorganisms to different food-use approved materials such as metals, rubbers, and polymers. For instance, *L. monocytogenes* strain 10403S showed a strong adhering capacity to 17 different materials after two hours contact (Beresford, Andrew, & Shama, 2001). *Salmonella enterica* ser. Typhimurium showed attachment to AISI 316 stainless steel surfaces (Schlisselberg & Yaron, 2013). Other research showed the impact of cross-contamination during food processing. For example, beef carcasses can get contaminated with *E. coli* O157:H7 during the slaughtering, dressing, chilling, or other stages of the meat process. These cells attached to the beef-contact surface (e.g. stainless steel or HDPE surfaces) found in meat facilities may serve as a source of cross-contamination (Dourou, Beauchamp, Yoon, Geornaras, Belk, Smith, et al., 2011).

1.1.2. Decreasing foodborne illness through sanitation

To minimize foodborne outbreaks, different organizations are involved in risk analysis regarding food safety in the United States including but not limited to: Codex Alimentarius Commission (CODEX), US Department of Agriculture (USDA), Center for Disease Control (CDC), Environmental Protection Agency (EPA), US Food and Drug Administration's (FDA). The last one regulates much of the US food market worth around $417 billion annually and $49 billion of imported products (Adley & Ryan, 2016). The CDC reported in 2011 that viruses (59%), bacteria (39%), and parasites (2%) caused the majority of foodborne illnesses (Scallan, et al., 2011).

Food safety is a concern for all individuals involved in the food supply chain. The management of food safety risk and food regulations are imperative to protect public health. In the United States, federal, state, and local regulatory agencies manage the retail food segment and other food safety issues. The USDA and FDA primarily regulate the safety of foods in interstate commerce through the Code of Federal Regulations.

One well-structured strategy to decrease foodborne disease is the implementation of a Food Safety Plan which is a set of written documents that incorporates a hazard analysis, preventive controls, supply-chain program, and a recall plan (Barach, et al., 2016). Establishing a Food Safety Plan involves a systematic process to ensure the safety of the food products. It starts with Hazard Analysis and Critical Control Points (HACCP), which is a quality control system that minimizes safety risks. It has been widely used in food production by controlling possible hazards throughout processing instead of emphasizing only the final product assessment (Allata, Valero, & Benhadja, 2017). The HACCP system focuses on hazard preventing actions. Factors affecting food safety should be monitored, such as changes in temperature, humidity, pH, O_2, CO_2, etc., in order to maintain the safety of products at every stage. The implementation of this system depends on extensive verification and validation. Internationally HACCP is recognized as a scientific approach to assess hazards involved with food production and determine control systems to ensure food safety by controlling food-borne diseases (Allata, Valero, & Benhadja, 2017; Kafetzopoulos, Psomas, & Kafetzopoulos, 2013).

Once hazards are identified, preventive controls (process, sanitation, supply chain, and/or allergen controls) are established to prevent them. Sanitation controls are needed at the beginning of the food production operation. Without a clean facility, equipment and the environment can introduce potentially hazardous contamination (Barach, et al., 2016). It is well known that fresh fruits and vegetables can be a vehicle for foodborne disease outbreaks around the world. Becoming one of the most prevalent interest factors in public health because they can be contaminated easily. This might be due to the deficiency in hygienic practices during harvesting or processing. Lack of effective sanitation preventive controls has contributed to major recalls (Arango, Rubino, Auras, Rachford, Bai, Grzesiak, et al., 2014; Sun, Baldwin, & Bai, 2019).

To improve food safety hazard transfer from unsanitary objects, and from personnel to food, food packaging material, and other food contact surfaces must be prevented. The cleanliness of food-contact surfaces is a primary focus for sanitation and preventive controls. Nonetheless, to prevent microbial cross-contamination, both food-contact and non-food contact surfaces are required to be considered. The most common method to decontaminate food products and surfaces is by the use of sanitizers, which reduce the level of pathogens after the surfaces were previously cleaned and rinsed. Any substance or mixture of substances that significantly reduce - but not destroy nor eliminate - the bacteria population on the inanimate surfaces are known as sanitizers, and must be approved for use by EPA, and regulated by FDA (Code of Federal Regulations Title 21. Part 178). (EPA, 1999; FDA, 2019b)

Sanitizers have a reported microbiological reduction of at least 99% of initial population at different efficacy and routines applied (Olanya, Annous, & Taylor, 2015). Sanitization of food contact or non-contact surfaces is a common practice in the industry; some include liquid sanitizers, for instance: chlorine, sodium hypochlorite, peracetic acid, hydrogen peroxide, ozone, and quaternary ammonium compounds (Tuladhar, Hazeleger, Koopmans, Zwietering, Beumer, & Duizer, 2012). Liquid sanitizers are used in industries to sanitize surface safter cleaning, but are limited by their efficacy of penetration to reach deeply to localized microorganisms into surfaces. Lately, gaseous sanitizers have been shown to have increased penetration capability and ability to reach inaccessible spots (Shynkaryk, Pyatkovskyy, Mohamed, Yousef, & Sudhir, 2015).

1.2. Chlorine dioxide

Chlorine dioxide (ClO_2) was discovered in 1811 by Sir Humphrey Davy and was known as the green-yellow gas euchlorine (Aieta & Berg, 1986). ClO_2 is a synthetic gas with powerful oxidant capacity that acts over a wide-ranging temperature and pH (Sun, Baldwin, & Bai, 2019). ClO_2 gas can be used for the decontamination of facilities and equipment because of its extensive antimicrobial spectrum (EPA, 1999; FDA, 2019a). It has been recognized for its disinfectant properties since the early 1990s. In 1967, the United States Environmental Protection Agencies (EPA) registered the liquid form of ClO_2 for use as a sanitizer, and in 1988 registered the gaseous form as a sterilant agent (A. Schaub, T. Hargett, Kamrud, R. Sterling, & Marshall, 1993).

ClO_2 species can be found in two different forms. The symmetric chlorine dioxide (OClO)has been widely used in the industry as a moderately strong oxidant. Another isomer was found as asymmetric chlorine dioxide (ClOO), so-called chlorine peroxide that is extremely kinetically unstable (Ganiev, Timergazin, Kabalnova, Shereshovets, & Tolstikov, 2005; Mueller & Willner, 1993). The symmetric isomer of chlorine dioxide is a green-yellow gas and has an odor similar to chlorine. The boiling point of ClO_2 is 11°C, and the density (liquid phase) is 1.653 g/cm^3 at 5°C. It is known to be soluble in water, acetic and sulfuric acids, carbon tetrachloride, and some other organic solvents (Gates, 1998; Mueller & Willner, 1993; Netrami, 2011; Sander, 2015).

ClO_2 is always generated on-site because of the risk of rapid decomposition. It is produced in strong acid solutions from sodium chlorite or sodium chlorate. In small to medium-scale industrial production where high purity and lower amounts are required, such as water treatment or food application, sodium chlorite is used as input. Sodium chlorite also reacts with chlorine gas to form ClO_2 gas. The chemistry is very complex, however, the equation describing the formation of the chlorine dioxide is generally written as:

$$2\ NaClO_2 + Cl_2 \rightarrow 2\ ClO_2 + 2NaCl \qquad (1.2.1)$$

The equation 1.2.1 describes principal reaction, where chlorine gas reacts directly with sodium chlorite. This reactions has a 100% theoretical molar conversion of chlorite (Gates, 1998; J. Taylor, Wohlers, & Amata, 2004).

1.2.1. Antimicrobial activity

Chlorine dioxide is a strong antimicrobial agent against multiple pathogenic microorganisms such as bacteria, viruses, and protozoans. It is highly effective at short treatment times and relatively low concentrations. It is recognized as a strong oxidizer and it is reported that ClO_2 has an oxidation capacity more than 2.5 times greater than the chlorine, based on the percent active chlorine. The chlorine atom in chlorine dioxide has an oxidation number of +4, and a reduction to chloride results in a gain of five electrons. Based on Equation 1.2.7 it can be said that one mole of ClO_2 contains 263% available chlorine, considering the amount of ClO_2 needed to achieve an equal bleaching power of 35.45 grams of chlorine since chlorine has a reference bleaching potential of 100% for its molecular weight (Ganiev, Timergazin, Kabalnova, Shereshovets, & Tolstikov, 2005).

$$\frac{5e^- \times 35.45\ \mathrm{gCl/mol}}{67.45\ \mathrm{g\ ClO_2/mol}} \approx 263\% \qquad (1.2.2)$$

ClO_2, unlike other chlorine-based sanitizers, does not form any trihalomethanes (THMs) or any halogenated organic compounds, known to be carcinogenic. ClO_2 has been recognized as having a greater efficiency at broad pH range from alkali to acid environment, in ranges between 5 to 10. Despite chlorine, ClO_2 becomes even more effective as the pH increases, as illustrated in Figure 1. In this study, multiple concentrations of chlorine and ClO_2 were added to solutions containing 15,000 viable cells of *E. coli* at pH of 6.5 and 8.5. In the x-axis the time needed to achieved 99% reduction of the population was recorded (Gates, 1998). However, one disadvantage to be considered for practical application includes its instability and the equipment needed for in situ production (WHO, 1999).

ClO_2 inactivates pathogenic microorganisms through the destabilization of cell membranes, interruption of protein synthesis, and oxidation of DNA, RNA, and proteins, showed in Figure 2. The main antimicrobial mechanism is due to reaction with the oxygenated compounds and proteins in the cell membranes allowing metabolic disruption (Sun, Baldwin, & Bai, 2019). The molecular size of the gas is known to be small (0.124 nm) (Chai, Hwang, Huang, Wu, & Sheen, 2020), this facilitates the penetration into bacterial cell membranes.

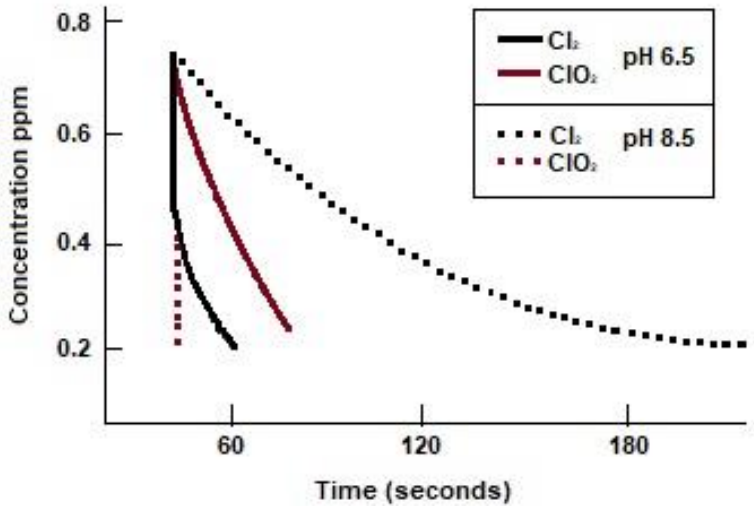

Figure 1. The effect of pH on aqueous solution of chlorine and chlorine dioxide at different concentration required to kill 99% of solutions containing 15,000 viable cells of *E. coli* at pH of 6.5 and 8.5. Adapted from (Gates, 1998)

ClO_2 disinfects by oxidation through the one-electron transfer mechanism, resulting in a reduction to ClO_2^-. The mechanism can be summarized in two possible primary actions. The inactivation may be reached by allowing permeability of the cell membrane by changing the configuration of lipids and protein which involve the oxidation of amino acids by the gas. The second option is due to the reaction with nucleic acid and/or protein structures. This principle remains incompletely understood. However, some research showed degradation in viral RNA, inducing genotoxicity or discontinuing replication of genome information. Both ways lead to the functional disruption of the synthesis of biochemically important compounds such as protein or genome information (Sun, Baldwin, & Bai, 2019).

Generally, the gaseous phase was more effective towards Gram-negative than Gram-positive bacteria. This as a result of the thickness on the peptidoglycan layer, Gram-negative bacteria have a thinner layer. Meanwhile, mold and yeast showed intermediate tolerance. Overall, the main factors that need to be a consideration to deactivate a specific microorganism in a certain food are: concentration, treatment time, temperature, and relative humidity (Sun, Baldwin, & Bai, 2019). The antimicrobial effect can be increased directly at a longer treatment time.

Additionally, the antimicrobial activities are reported to be enhanced at higher temperatures, which can be due to a higher diffusion coefficient for the gaseous

phase of the ClO_2. (Lee, Burgess, Rubino, & Auras, 2015; Netrami, 2011). Another factor that increased the effectiveness is the relative humidity. At higher relative humidity, a greater reduction of pathogen population was reported. This might be explained due to the increment of the pores' sizes in the bacteria due to swelling at high humidity, which allow penetration of the ClO_2 molecule into the bacteria. This penetration interferes with intracellular respiration and enhances the deterioration of the trans-membrane ionic gradient (Arango, et al., 2014; Lee, Burgess, Rubino, & Auras, 2015; Sun, Baldwin, & Bai, 2019; Sy, McWatters, & Beuchat, 2005).

Some authors reported that this gas is effective on biofilms such *as B. cereus*, *L. monocytogenes*, and *E. coli* O157:H7. A biofilms is an accumulation of a microorganism (or many different) in a matrix of extracellular polymeric substances. The effectiveness at reaching and inactivating pathogenic cells within a biofilm is due to its high diffusivity and penetration ability. (Netrami, 2011; Sun, Baldwin, & Bai, 2019). Although ClO_2 gas is an effective antimicrobial agent, the change on the physical and chemical properties of the food or material due to the exposure to the gas is a concern. Several studies have reported the antimicrobial effects of both aqueous and gaseous ClO_2 against pathogenic microorganisms, as listed in Table 1.

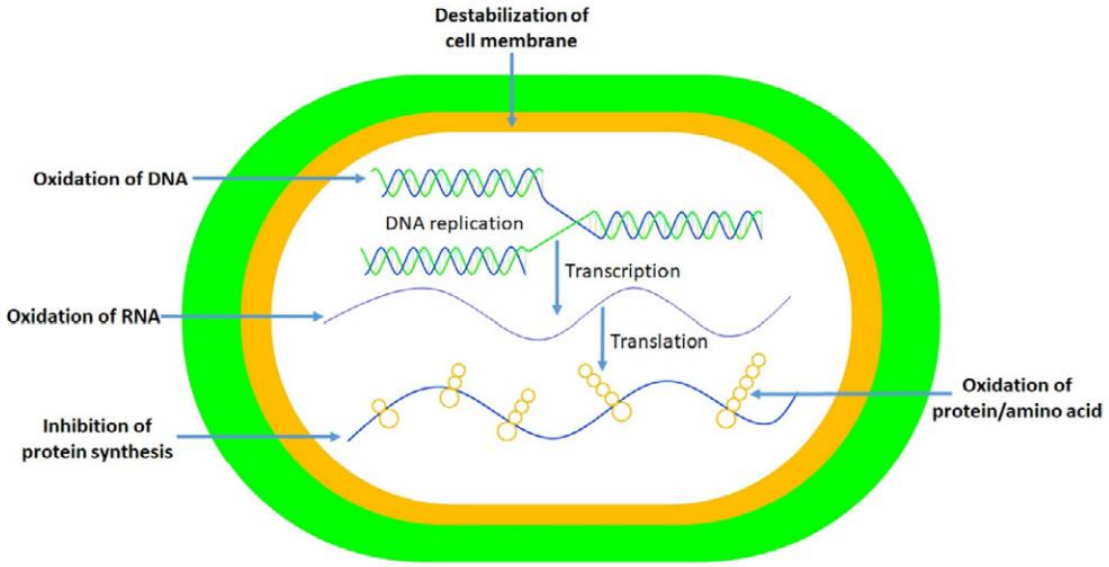

Figure 2. Mechanism of action of Chlorine Dioxide against pathogenic microorganisms. Adapted from (Sun, Baldwin, & Bai, 2019)

Some experiments have been conducted on visual appearance, specifically the surface color in food products, such as browning, which is caused by the production of melanin (Walker & Ferrar, 1998). Gaseous ClO_2 showed a negative impact on treated fruits and vegetables through enzymatic browning formation. This browning affects the appearance and organoleptic properties and is related to the deterioration of nutritional quality. However, additional treatments can be added to the gas exposure to inhibit browning, such as immersion for 1 min in a 0.5% solution of HCl L-cysteine monohydrate. (Fu, Zhang, Wang, & Du, 2007; Gómez-López, Ragaert, Jeyachchandran, Debevere, & Devlieghere, 2008; Saengnil, Chumyam, Faiyue, & Uthaibutra, 2014). Other authors reported a negative color change in spinach leaves, which occurred during storage after being exposed even to 50 ppm of gaseous ClO_2 (Park & Kang, 2015). Also, treatments with higher concentrations may lead to bleaching of fruits and vegetables (Singh, Singh, Bhunia, & Stroshine, 2002; Sy, McWatters, & Beuchat, 2005).

1.2.2. Photochemical dissociation

One of the concerns regarding the use of this compound is its photochemical sensitivity. The excitation wavelengths of ClO_2 are near the ultraviolet and visible light. This excitation leads to dissociation into ClO + O or Cl + O_2 (Davis & Lee, 1996). Some experimental results indicate the photochemical decomposition of ClO_2 is explained by:

$$OClO + hv \rightarrow ClO + O \qquad (I)$$
$$OClO + hv \rightarrow ClOO \rightarrow Cl + O_2 \qquad (II)$$
$$OClO + hv \rightarrow Cl + O_2 \qquad (III)$$

where, the photon energy is given by Planck's constant *h* multiplied by the frequency of the light *v*. The excitation of OClO (symmetrical isomer) leads to one of the following three pathways (Davis & Lee, 1996; Vaida & Simon, 1995):

(I) Photochemical dissociation into ClO + O
(II) Photoisomerization to form asymmetrical isomer ClOO, to further thermally dissociate into atomic Cl + O_2 known as asymmetrical process
(III) Photochemical dissociation into atomic Cl + O_2 known as symmetrical process

Table 1. Summary of research studies on antimicrobial efficiencies of chlorine dioxide for food products

Microorganism	Food Product	Phase	Concentration	Times	Log 10 reduction	Reference
B. cereus	Apple	Aqueous	200 um/mL	5 min	≤ 3.79 log CFU/fruit	(Kreske*, et al.*, 2006)
E. coli	Apple	Gas	0.03 - 0.30 ppm	1 - 20 h	≤ 5 log CFU/g	(Sapers*, et al.*, 2003)
E. coli	Tomato	Gas	0.01 mg/L	14 d	≤ 4.7 log CFU/g	(Sun*, et al.*, 2017)
E. coli O157:H7	Alfalfa seed	Aqueous	10 - 50 mg/L	3-10 min	≤ 1.22 log CFU/g	(Singh 2003)
E. coli O157:H7	Alfalfa sprout	Aqueous	50 mg/L	10 min	≤ 3.96 log CFU/g	(Kim*, et al.*, 2009)
E. coli O157:H7	Apple	Gas	3-12 mg/L	10-30 min	≤ 8 log CFU/site	(Du*, et al.*, 2003)
E. coli O157:H7	Apple	Aqueous	3-5 ppm	5 min	≤ 5 log CFU/g	(Rodgers*, et al.*, 2004)
E. coli O157:H7	Blueberries	Gas	4 mg/L	12 h	4.5 log CFU/g	(Popa*, et al.*, 2007)
E. coli O157:H7	Cabbage	Gas	1.4 - 4.1 mg/L	6 - 21 min	≤ 3.13 log CFU/g	(Rodgers*, et al.*, 2004)
E. coli O157:H7	Cantaloupe	Aqueous	3 - 5 ppm	5 min	≤ 5 log CFU/g	(Rodgers*, et al.*, 2004)
E. coli O157:H7	Carrot	Aqueous	5 - 20 mg/L	1-15 min	≤1.39 log CFU/g	(Singh*, et al.*, 2002)
E. coli O157:H7	Carrot	Gas	0.5 - 1 mg/L	5 - 15 min	≤ 3.08 log CFU/g	(Singh*, et al.*, 2002)
E. coli O157:H7	Carrot	Gas	1.4 - 4.1 mg/L	6 - 21 min	≤ 5.62 log CFU/g	(Sy*, et al.*, 2005)
E. coli O157:H7	Green pepper	Gas	0.15 - 1.5 mg/L	30 min	≤ 7.3 log CFU/pepper	(Han*, et al.*, 2000)
E. coli O157:H7	Lettuce	Aqueous	3-5 ppm	5 min	≤ 5 log CFU/g	(Rodgers*, et al.*, 2004)
E. coli O157:H7	Lettuce	Gas	4.3 - 8.7 mg/L	30 - 180 min	≤ 6.9 log CFU/g	(Lee*, et al.*, 2004)
E. coli O157:H7	Lettuce	Aqueous	5 - 50 ppm	10 min	≤ 1.44 log CFU/g	(Kim*, et al.*, 2008)

Table 1. Continued

Microorganism	Food Product	Phase	Concentration	Times	Log 10 reduction	Reference
E. coli O157:H7	Lettuce	Aqueous	3 - 5 ppm	5 min	≤ 5 log CFU/g	(Rodgers, *et al.*, 2004)
E. coli O157:H7	Lettuce	Gas	1.4 - 4.1 mg/L	6 - 21 min	≤ 1.57 log CFU/g	(Sy, *et al.*, 2005)
E. coli O157:H7	Lettuce	Aqueous	5 - 20 mg/L	1 - 15 min	≤ 0.90 log CFU/g	(Singh, *et al.*, 2002)
E. coli O157:H7	Lettuce	Gas	0.5 - 1 mg/L	5 - 15 min	≤ 2.31 log CFU/g	(Singh, *et al.*, 2002)
E. coli O157:H7	Spinach leaves	Gas	0.13 mg/L	20 min	1.25 - 2.54 log CFU/g	(Park and Kang 2015)
E. coli O157:H7	Spinach leaves	Gas	0.03 mg/L	10 min	3.4 log CFU/g	(Park and Kang 2015)
E. coli O157:H7	Strawberries	Aqueous	3 - 5 ppm	5 min	≤ 5 log CFU/fruit	(Han, *et al.*, 2004)
E. coli O157:H7	Strawberries	Gas	0.2 - 4 mg/L	15 - 30 min	≤ 5 log CFU/fruit	(Han, *et al.*, 2004)
E. coli O157:H7	Strawberries	Gas	0.6 - 3 mg/L	10 min	≤ 5 log CFU/fruit	(Lukasik, *et al.*, 2003)
E. coli O157:H7	Strawberries	Aqueous	100 - 200 ppm	2 min	≤ 2 log CFU/fruit	(Unda, *et al.*, 2003)
E. coli O157:H7	Tomato	Gas	0.03 mg/L	20 min	3.9 log CFU/g	(Park and Kang 2015)
L. monocytogenes	Alfalfa sprout	Aqueous	50 mg/L	10 min	≤ 2.36 log CFU/g	(Kim, *et al.*, 2009)
L. monocytogenes	Apple	Aqueous	3 - 5 ppm	5 min	≤ 5 log CFU/g	(Rodgers, *et al.*, 2004)
L. monocytogenes	Apple	Gas	4 mg/L	10 min	≤ 3.2 log	(Du, *et al.*, 2002)
L. monocytogenes	Cantaloupe	Aqueous	3 - 5 ppm	5 min	≤ 5 log CFU/g	(Rodgers, *et al.*, 2004)
L. monocytogenes	Carrot	Gas	1.4 - 4.1 mg/L	10 - 29 min	≤ 5.88 log CFU/g	(Sy, *et al.*, 2005)
L. monocytogenes	Lettuce	Aqueous	3 - 5 ppm	5 min	≤ 5 log CFU/g	(Rodgers, *et al.*, 2004)

Table 1. Continued

Microorganism	Food Product	Phase	Concentration	Times	Log 10 reduction	Reference
L. monocytogenes	Lettuce	Gas	4.3 - 8.7 mg/L	30 - 180 min	≤ 5.4 log CFU/g	(Lee ,*et al.* 2004)
L. monocytogenes	Lettuce	Aqueous	3 - 5 ppm	5 min	≤ 5 log CFU/g	(Rodgers,*et al.* 2004)
L. monocytogenes	Lettuce	Aqueous	5 - 50 ppm	10 min	≤ 1.20 log CFU/g	(Kim,*et al.* 2008)
L. monocytogenes	Lettuce	Gas	1.4 - 4.1 mg/L	10 - 29 min	≤ 1.53 log CFU/g	(Sy,*et al.* 2005)
L. monocytogenes	Lettuce	Aqueous	3 - 5 ppm	5 min	≤ 5 log CFU/g	(Rodgers,*et al.* 2004)
L. monocytogenes	Spinach leaves	Gas	0.13 mg/L	20 min	1.25 - 2.54 log CFU/g	(Park and Kang 2015)
L. monocytogenes	Spinach leaves	Gas	0.03 mg/L	10 min	3.4 log CFU/g	(Park and Kang 2015)
L. monocytogenes	Strawberries	Gas	0.2 - 4 mg/L	15 - 30 min	≥ 5 log CFU/g	(Han,*et al.* 2004)
L. monocytogenes	Strawberries	Gas	0.6 - 3 mg/L	10 min	≥ 5 log CFU/g	(Han,*et al.* 2004)
Lactic acid bacteria	Rib eye steak	Aqueous	30 - 100 ppm	2 min	≥ 1 log CFU/ cm^2	(Unda,*et al.* 2006)
Molds	Blueberries	Gas	4 mg/L	12 h	≤ 3.0 log CFU/g	(Popa,*et al.* 2007)
Molds	Potato	Aqueous	9 ppm	30 - 300 min	≤ 0.9 log CFU/fruit	(Park,*et al.* 2008)
Salmonella enterica	Tomato	Gas	0.15 - 0.85 mg/L	58 min	7.37 log CFU/g	(Nematri,*et al.* 2016)
Salmonella enterica	Tomato	Gas	8 mg/L	60 s	2.94 log CFU/g	(Trinetta,*et al.* 2010)
Salmonella enterica	Tomato	Gas	10 mg/L	120 s	3.86 log CFU/g	(Trinetta,*et al.* 2010)
Salmonella enterica	Tomato	Gas	10 mg/L	180 s	4.87 log CFU/g	(Trinetta,*et al.* 2010)

Table 1. Continued

Microorganism	Food Product	Phase	Concentration	Times	Log 10 reduction	Reference
Salmonella enterica	Tomato	Gas	0.4 mg/L	4 h	4.6 - 5 log CFU/g	(Olanya, *et al.* 2015)
Salmonella Montevideo	Strawberries	Aqueous	100 - 200 pmm	2 min	≤ 2 log CFU/fruit	(Lukasik, *et al.* 2003)
Salmonella spp.	Apple	Gas	1.4 - 4.1 mg/L	6 - 25 min	≤ 4.21 log CFU/g	(Huang, *et al.* 2006)
Salmonella spp.	Bell pepper	Gas	100 mg/L	1 h	≤ 5.97 log CFU/fruit	(Yuk, *et al.* 2006)
Salmonella spp.	Blueberries	Gas	8 mg/L	120 min	≤ 3.67 log CFU/g	(Sy, *et al.* 2005)
Salmonella spp.	Blueberries	Gas	4 mg/L	12 h	3.8 log CFU/g	(Popa, *et al.* 2007)
Salmonella spp.	Cabbage	Gas	1.4 - 4.1 mg/L	10 - 31 min	≤ 4.42 log CFU/g	(Sy, *et al.* 2005)
Salmonella spp.	Carrot	Gas	1.4 - 4.1 mg/L	10 - 31 min	≤ 5.15 log CFU/g	(Sy, *et al.* 2005)
Salmonella spp.	Lettuce	Gas	1.4 - 4.1 mg/L	10 - 31 min	≤ 1.58 log CFU/g	(Sy, *et al.* 2005)
Salmonella spp.	Mungbean sprout	Gas	0.5 mg/L	15 min	3 log CFU/g	(Prodduk, *et al.* 2014)
Salmonella spp.	Mungbean sprout	Gas	0.5 mg/L	30 min	3 - 4 log CFU/g	(Prodduk, *et al.* 2014)
Salmonella spp.	Mungbean sprout	Gas	0.5 mg/L	60 min	4 - 5.5 log CFU/g	(Prodduk, *et al.* 2014)
Salmonella spp.	Onion	Gas	1.4 - 4.1 mg/L	10 - 29 min	≤ 1.94 CFU/g	(Sy, *et al.* 2005)
Salmonella spp.	Peach	Gas	1.4 - 4.1 mg/L	5 - 20 min	≤ 3.23 log CFU/g	(Sy, *et al.* 2005)
Salmonella spp.	Raspeberries	Gas	4 - 8 mg/L	30 - 120 min	≤ 1.54 log CFU/g	(Sy, *et al.* 2005)

Table 1. Continued

Microorganism	Food Product	Phase	Concentration	Times	Log 10 reduction	Reference
Salmonella spp.	Strawberries	Gas	4 - 8 mg/L	30 - 120 min	≤ 3.76 log CFU/g	(Sy, *et al.* 2005)
Salmonella spp.	Tomato	Gas	1.4 - 4.1 mg/L	5 - 20 min	≤ 4.33 log CFU/g	(Sy, *et al.* 2005)
Salmonella spp.	Tomato	Aqueous	5 ppm	10 - 60 s	≤ 5.6 log CFU/cm^2	(Pao, *et al.* 2009)
Salmonella spp.	Tomato	Gas	0.03 mg/L	20 min	3.5 log CFU/g	(Park and Kang 2015)
Salmonella Typhimurium	Alfalfa sprout	Aqueous	50 mg/L	1 - 10 min	≤ 2.23 log CFU/g	(Kim, *et al.* 2009)
Salmonella Typhimurium	Lettuce	Gas	4.3 - 8.7	30 - 180 min	≤ 5.4 log CFU/g	(Lee, *et al.* 2004)
Salmonella Typhimurium	Lettuce	Aqueous	5 - 50 ppm	10 min	≤ 1.95 log CFU/g	(Kim, *et al.* 2008)
Salmonella Typhimurium	Potato	Aqueous	9 ppm	30 - 300 min	≤ 1.9 log CFU/fruit	(Park, *et al.* 2008)
Yeast	Blueberries	Gas	4 mg/L	12 h	3.2 log CFU/g	(Popa, *et al.* 2007)
Yeast	Potato	Aqueous	9 ppm	30 - 300 min	≤ 1.1 log CFU/fruit	(Park, *et al.* 2008)
Yeast & Molds	Apple	Gas	1.4 - 4.1 mg/L	6 - 25 min	≤ 1.68 log CFU/g	(Sy, *et al.* 2005)
Yeast & Molds	Blueberries	Gas	4 - 8 mg/L	30 - 120 min	≤ 2.78 log CFU/g	(Sy, *et al.* 2005)
Yeast & Molds	Grapefuit	Gas	14.5 mg/L	10 d	0.95 log CFU/g	(Sun, *et al.* 2017)
Yeast & Molds	Onion	Gas	1.4 - 4.1 mg/L	5 - 20 min	≤ 0.22 log CFU/ g	(Sy, *et al.* 2005)
Yeast & Molds	Peach	Gas	1.4 - 4.1 mg/L	5 - 20 min	≤2.65 log CFU/ g	(Sy, *et al.* 2005)
Yeast & Molds	Raspeberries	Gas	4 - 8 mg/L	30 - 120 min	≤3.18 log CFU/ g	(Sy, *et al.* 2005)
Yeast & Molds	Strawberries	Gas	4 - 8 mg/L	30 - 120 min	≤4.16 log CFU/ g	(Sy, *et al.* 2005)
Yeast & Molds	Tomato	Gas	1.4 - 4.1 mg/L	6 - 25 min	≤ 1.16 log CFU/ g	(Sy, *et al.* 2005)

ClO_2 showed excitation at different Photon's energy, which is related to the frequency of the electromagnetic radiation. The photodissociation pathway was found to be wavelength-dependent in a gas phase. (Davis & Lee, 1996; Mueller & Willner, 1993; Vaida & Simon, 1995). The movement from the ground state to excited state at different wavelengths is shown in Figure 3, where the excitation occurred between 350 and 475 nm. Additionally, ClO_2 is more likely to dissociate at wavelengths shorter than 380 nm (UV light region) to ClO + O and proceeds via a direct mechanism. The excitation of ClO_2 can lead to any of the three pathways described above. In gas-phase at excitation energies above 3.1 eV (wavelength lower than 380 nm) the transition to the excited state indicated a lifetime ranging from 2×10^{-7} μs to 2×10^{-5} μs, and photochemical dissociation to form ClO + O and Cl + O_2. (Davis & Lee, 1996; Vaida & Simon, 1995). However, dissociation at wavelengths larger than 380nm (visible light region) occurs by an indirect mechanism. The ClOO produced from the excitation of OClO remains in water. This is useful to assure stability during application. Nonetheless, dark conditions are always considered to minimize photodissociation (Davis & Lee, 1996; Mueller & Willner, 1993; Vaida & Simon, 1995).

Figure 4 shows a representation of the overall photodissociation of OClO, where $^2B_1$ is the ground state, and $^2A_2$ represents the excited stated. Once the molecules reach the excited stated, it decreases its bond angles (117.9° to 106.4°) followed by a spin-orbit coupling, which causes an increase in bond angles of the OClO ($^2A_1$). From $^2A_1$, the molecules can dissociate into ClO + O, or Cl + O2. However, the molecules might also convert into $^2B_2$ through the vibronic coupling, which results in a decrease in the bond angle (120° to 90°). This vibrational relaxation allows a third pathway known as asymmetrical process described above (Vaida & Simon, 1995).

In solutions, vibrational relaxation and internal conversion occur more rapidly than photoreactions; hence, dissociation will happen from the $^2B_2$ excited state. OClO in water forms HCl and $HClO_3$; the chemistry observed in solution is independent of excitation wavelength, where 90% of the excited molecules of the solution dissociate into ClO + O and the remaining 10% generate Cl + O_2 (Davis & Lee, 1996; Vaida & Simon, 1995).

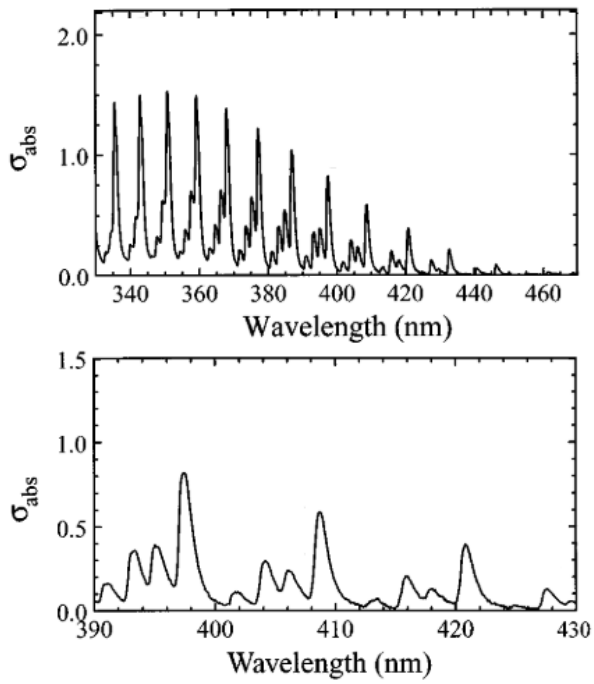

Figure 3. OClO absorption spectrum. Upper figure: OClO absorbance' peaks. Lower figure: OClO vibrational near to 400 nm. Adapted from (Davis & Lee, 1996).

1.2.3. Solubility in water

ClO_2 gas is highly soluble in water, and solubility is inversely related to temperature. In other words, as the temperature increases, the solubility decreases. Literature suggests that the water solubility of ClO_2 is about 3000 mg/L at 25°C (J. Taylor, Wohlers, & Amata, 2004). However, ClO_2 solutions have been made at concentrations up to 60,000 mg/L. This is explained by the off-gassing at all concentrations, which is proportional to the solution concentration; additionally, liquid solutions at higher concentrations are highly unstable. These properties allow ClO_2 at higher concentrations than 3 g/L to be easily released from the matrix with agitation, meanwhile in lower concentrations, ClO_2 is more difficult to remove (Gates, 1998).

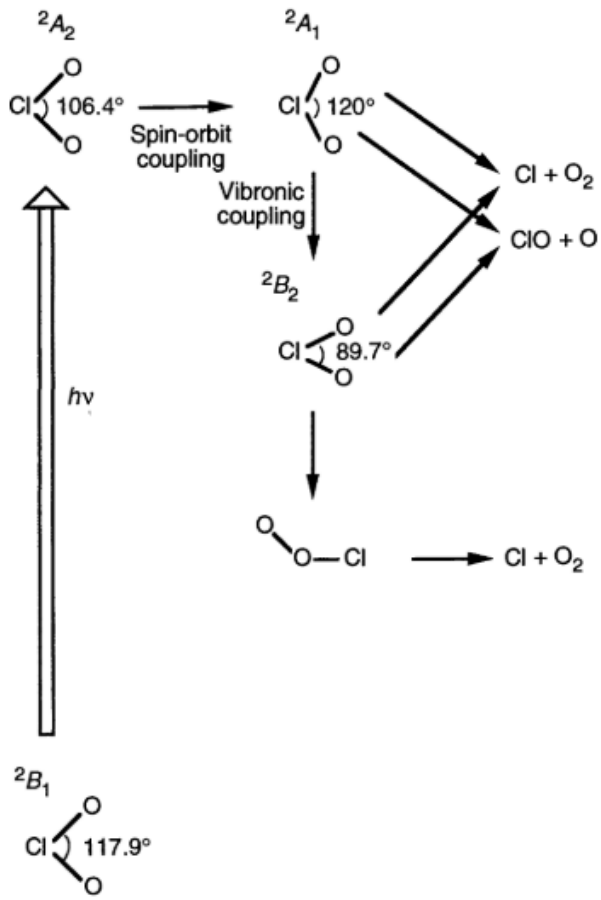

Figure 4. Schematic representation of the photo reactivity of OCIO in gas-phase. Adapted from (Vaida & Simon, 1995).

To understand the distribution and interaction between gas and liquid phases, it is important to know Henry's law, which states the equilibrium ratio between the abundances in the gas phase and the aqueous phase is constant for a dilute solution. The principle of this law establishes that the amount of dissolved gas in water is proportional to its partial pressure in the gas phase. This proportionality fraction is called Henry´s law constant, usually denoted as H^{cp} (mol m^{-3} Pa^{-1}). The value of H^{cp} is reported as 1×10^{-2} mol · m^{-3} · Pa^{-1}(Gates, 1998; Sander, 2015).

Henry´s law solubility is often defined as:

$$H^{cp} = \frac{Ca}{p} \tag{1.2.3}$$

Here, *Ca* (mol m^{-3}) is the concentration of a species in the aqueous phase, and *p* is the partial pressure (Pa) of that same species in the gas phase under equilibrium conditions. Henry´s law equation can also be expressed as the dimensionless ratio between the aqueous phase concentrations *Ca* (mol m^{-3}) of a species and its gas phase concentration, *Cg* (mol m^{-3}). The dimensionless ratio is denoted as H^{cc}.

For an ideal gas, the conversion can be defined as:

$$H^{cc} = H^{cp} x\, RT = \frac{Ca}{Cg} \qquad (1.2.4)$$

where R is the gas constant (8.3145 m^3 Pa mol^{-1} K^{-1}) and *T* (K) is temperature. Sometimes, this dimensionless constant is called the "water–air partitioning coefficient." The ratio will remain constant as long as the temperature and pressure in the environment remain the same (Sander, 2015).

ClO_2, at 23°C, and under equilibrium conditions, has been reported to be about 23 times more concentrated in aqueous phase than in the gas phase (Gates, 1998). Additionally, using the H^{cc} equation, it can be calculated that at 298.15 K (25°C), the ratio is about 25. In other words, Ca is 25 times greater than Cg (Sander, 2015; Taube & Dodgen, 1949).

1.2.4. Diffusion coefficient properties

In general, the gas phase of a substance has a higher penetration ability than the aqueous phase within surface irregularities. In dilute species transport, molecular movement is due to diffusion properties linked to the species involved, and the physical property known as diffusion coefficient. The movement goes from a higher concentration region to a lower concentration of a specific species. This molecular transport of one substance relative to another is determined as diffusion. This mass transport is also known as mass diffusion, concentration diffusion, or even ordinary diffusion. This movement is typically explained by Fick´s first law (Bird, Stewart, & Lightfoot, 2006).

The mass flux is defined as:

$$\mathbf{J}_A = \boldsymbol{\rho}\, \boldsymbol{x}\, D_{AB} * \boldsymbol{\nabla \omega}_A \qquad (\mathbf{1.2.5})$$

where, J_A is mass flux. The mass flux is described as the mass flow rate of specie A per unit area (cross sectional area), ρ is the density of the system (chlorine dioxide – air), D_{AB} is the Diffusion coefficient of substance A in B, and ω_A is the mass fraction of the species A. In a low density system, the most common type involves air as species B. At steady state, the mass flow is directly proportionally to the diffusion coefficient, and the gradient of concentration. Hence, the intrinsic properties that will determine the overall molecular movement in a space is the diffusivity, also known as diffusion coefficient (Bird, Stewart, & Lightfoot, 2006).

The development of an equation for D_{AB} – considering species as rigid spheres of unequal masses and diameters – based on Chapman-Enskog kinetics was able to predict the diffusivity within a 5% accuracy. Then, the following equation was suggested, considering the behavior of the ideal gas, to obtain D_{AB} [cm^2/s]:

$$D_{AB} = 0.0018583 \sqrt[2]{\frac{T^3}{\pi} * \left(\frac{1}{M_A} + \frac{1}{M_B}\right)} * \frac{1}{P\ \sigma_{AB}^2 \Omega_{D_{AB}}} \qquad (1.2.6)$$

where, T is temperature [K] in which the system is at during the diffusion of species A, M is the molecular weight [g/mol] of the species, P is pressure in the system [atm], σ is the collision diameter [Å] and Ω, known as integrals collisions, is the dimensionless parameter based on the energy attraction of a pair of molecules. These last two are found in the Lennard-Jones potentials parameters (Bird, Stewart, & Lightfoot, 2006). These can be approximated based on properties, where $\sigma = 1.166\ \tilde{v}_b^{1/3}$, and $\tilde{v}$ = molecular volume [cm^3/g-mol] at boiling point temperature. Additionally, Ω can be found in a table for Leonard-Parameter collision integrals, which is closely related to ε/K, which is the maximum energy attraction between two pair of molecules within the same species and can be calculated as $\varepsilon/K = 1.15\ T_b$, and T_b is boiling point temperature [K] of a specific species (Bird, Stewart, & Lightfoot, 2006).

To calculate the diffusion coefficient for ClO_2 in air, both σ and ε/K are required. The first one can be estimated from the density and molecular weight of ClO_2. The density at 10°C is 1.614 g/mL, and its molecular weight is 67.452 g/mol (J. Taylor, Wohlers, & Amata, 2004), where $\tilde{v}$ can be obtained by dividing molecular weight by density ($\tilde{v}$ = 41.7918 cm^3/g-mol). Hence, σ for ClO_2 is 4.046 Å. The second parameter can be found based on the ClO_2 boiling point, which is 11°C (J. Taylor, Wohlers, & Amata, 2004). Hence, ε/K for ClO_2 is 326.7725K. These two parameters for water were 3.617 Å, and 97.0 K, respectively (Bird, Stewart, & Lightfoot, 2006).

Since the system consists of a mixture of ClO_2 and air, these parameters must be calculated for the mixture with the following equations:

$$\boldsymbol{\sigma}_{AB} = \frac{1}{2}(\boldsymbol{\sigma}_{B} + \boldsymbol{\sigma}_{A}) \qquad (1.2.7)$$

$$\frac{\boldsymbol{\varepsilon}_{AB}}{K} = \sqrt{\left(\frac{\boldsymbol{\varepsilon}_{B}}{K} * \frac{\boldsymbol{\varepsilon}_{B}}{K}\right)} \qquad (1.2.8)$$

The estimated value of the diffusion coefficient for ClO_2 will depend on these physical properties given by the species involved. Using these equations, the diffusion coefficients through air are estimated at 0.125, 0.114, and 0.136 cm^2/s at 23°C, 5°C and 40 °C, respectively. Meanwhile, ClO_2 diffusion coefficients in air were measured to be 0.145, 0.129, and 0.173 cm^2/s at 23°C, 5°C, and 40 °C, respectively (Lee, Burgess, Rubino, & Auras, 2015). The discrepancy between estimated and measured values might be because Lennard-Jones parameters were estimated as well, which could add an extra source to the values.

1.2.5. Analytical method to measure concentration

The reactive and unstable nature of ClO_2 gas diminish the possibility of a quick and accurate method to measure its concentrations. There are several methods that can lead to a measurement based on colorimetric methods, amperometric titration, thiosulfate titration, ion chromatography, toxic gas vapor detector tube, electrochemical gas sensor and spectrophotometer. Since the main applications of ClO_2 are in pulp production and waste water treatment, most of the methods were developed to determine the concentration in aqueous phase. Several methods require a specific solution in order to capture the gas and determine its concentrations, based on solubility. These solutions might be potassium iodide (KI), or distilled water. Additionally, the detection level of these methods are inefficient, therefore, larger volumes of gas are required (Kaczur & W. Cawlfield, 2000; J. Taylor, Wohlers, & Amata, 2004).

The colorimetric methods are widely used because of practicality and fairly good accuracy. These methods are based on the color formation due to DPD (N,N-diethyl-p-phenylenediamine). For this method, glycine is added prior to the reagent to convert free chlorine instantaneously into chloroaminoacetic acid but has no effect on ClO_2, then the color is assessed at approximately 515 nm. The

spectrophotometer method is based on the excitation of the gas from 385 to 670 nm, and the detector shows the concentration of the gas based on the absorbance and transmittance (Davis & Lee, 1996; Netrami, 2011). The molar absorptivity of ClO_2 (ε = 1,250 M^{-1} cm^{-1}) at its maximum absorbance wavelength (λ_{max} = 359 nm) can be used to calculate concentrations of a pure compound, based on the absorbance of a sample in a spectrophotometer. Commercially available UV-Vis spectrophotometers are used to measure changes in light intensity due to the interested compound's transmittance and absorbance (Gates, 1998).

CHAPTER II
ROLE OF WATER SOLUBILITY AND DIFFUSION IN MODELING THE GAS TRANSPORT INVOLVED IN SURFACE DECONTAMINATION WITH CHLORINE DIOXIDE GAS

This article hasn't been published anywhere, nor will it be before I turn in the final version of my ETD, so I didn't include a publication statement.

2.1. Abstract

ClO_2 is recognized as a strong antimicrobial agent against multiple pathogenic microorganisms found in produce and on hard surfaces involved in food processing. However, few studies have been conducted to address the depletion of gas by materials that might be present during the decontamination procedure, such as organic matter, aqueous films, and oil film. These data are important for the design of proper sanitization treatments, and to develop mathematical simulations to determine the time required for empirical studies. The objective was to develop a physics-based model to understand the transport of ClO_2 gas into stainless steel crevices during surface decontamination. A 680 mL stainless steel chamber was filled with ClO_2 gas to reach a concentration of 2500 ppm. The gas was circulated inside a closed chamber with three different volumes of deionized water (20, 40, and 60 mL), and 0 mL (control). The gas was monitored and recorded until the concentration dropped below the detection limit. The decay was modeled with two, first-order exponential reaction terms. A computer simulation model was developed and validated using reported experimental results in the literature, and the data obtained at the first stage of this experiment. This investigation showed a increase in the reaction rate from 0.026 1/h to 0.253 1/h, 1.206 1/h, and 0.595 1/h at different water volume 20, 40, and 60 mL, respectively, at a constant exposure surface area of 6.418×10^{-3} m^2. Additionally, an increase was shown from 0.025 1/h to 6.021 1/h, 2.791 1/h, and 3.720 1/h at a surface area of 18.19×10^{-3} m^2. Finally, an increase was shown from 0.025 1/h to 2.911 1/h, 3.331 1/h, and 6.838 1/h at a surface area of 2.16×10^{-3} m^2. A mathematical model was proposed for analyzing the time needed for ClO_2 gas to reach the bottom of a possible crevice during equipment surface decontamination. The simulation showed that the time needed is depth-dependent. The time needed for the gas to reach the bottom at depths of 1 and 10 was 0.15 and 15 seconds, respectively, at diffusion coefficient of 0.145 cm^2/s, and 0.22 and 25 seconds, respectively at diffusion coefficient of 0.097 cm^2/s. The model showed that at depth 100 mm, the initial concentration did not reach the bottom assuming the worst case reaction rate with water (6.838 1/h). This can help the food processing industry in constructing an effective gas sanitizing system and establishing optimum treatment conditions.

2.2. Introduction

Foodborne disease outbreaks result from the consumption of contaminated food. Contaminated food, like fresh fruits and vegetables have been identified as the main vehicle for illnesses because they can carry various harmful microorganisms. Other possible sources of contamination are mostly poor practices during food production, harvesting, preparation, and equipment cleaning, and the lack of good agricultural practices (Adley & Ryan, 2016). The U.S. Centers for Disease Control and Prevention estimates that each year around 9.4 million people get sick and 2600 deaths occur due to foodborne diseases (Scallan, et al., 2011). Food recalls have been a concern in the global food industry because they result in significant losses for food production, processing, and marketing firms. Food safety is a concern for all individuals involved in the food supply chain. The management of food safety risk and food regulations are imperative to protect public health. To minimize foodborne outbreaks, different organizations are involved in risk analysis regarding food safety in the United States including but not limited to: Codex Alimentarius Commission (CODEX), US Department of Agriculture (USDA), Center for Disease Control (CDC), Environmental Protection Agency (EPA), and US Food and Drug Administration's (FDA).

Sanitation controls are needed at the beginning of the food production operation. Without a clean facility, equipment and the environment can introduce potentially hazardous contamination (Barach, et al., 2016). It is well known that fresh fruits and vegetables can be a vehicle for foodborne disease outbreaks around the world. Lack of effective sanitation preventive controls has contributed to major recalls (Arango, et al., 2014; Sun, Baldwin, & Bai, 2019). Improve food safety practices are needed to prevent transfer of hazards from unsanitary objects and from personnel to food, food packaging material, and other food contact surfaces. The cleanliness of food-contact surfaces is a primary focus for sanitation and preventive controls. Nonetheless, to prevent microbial cross-contamination cleaning and sanitation of both food-contact and non-food contact surfaces must be considered. The most common method to decontaminate food products and surfaces is by the use of sanitizers, which reduce pathogens after the surfaces are previously cleaned and rinsed. Any substance or mixture of substances that significantly reduce - but not destroy nor eliminate - the bacteria population on the inanimate surfaces are known as sanitizers and must be approved by EPA to use, and regulated by FDA. Sanitizers have reported microbiological reduction to at least 99% of the initial population at different efficacy and routines applied (Code of Federal Regulations Title 21. Part 178). (EPA, 1999; FDA, 2019b; Olanya, Annous, & Taylor, 2015)

Sanitization of food contact or non-contact surfaces is a common practice in the industry; some include liquid sanitizers, for instance: sodium hypochlorite,

peracetic acid, hydrogen peroxide, aqueous ozone, quaternary ammonium compounds, chlorine, chlorine dioxide (ClO_2) among others (Tuladhar, Hazeleger, Koopmans, Zwietering, Beumer, & Duizer, 2012). Liquid sanitizers are used in industries to sanitize surfaces after cleaning, but are limited by their ability to reach microorganisms in deep surface crevices. The use of ClO_2 has become more attractive as a disinfectant due to its superior sanitizing efficacy compared to other sanitizers available.

ClO_2 is a strong antimicrobial agent against multiple pathogenic microorganisms such as bacteria, viruses, and protozoans. It is highly effective at short treatment times and relatively low concentrations (Ganiev, Timergazin, Kabalnova, Shereshovets, & Tolstikov, 2005). ClO_2, unlike other chlorine-based sanitizers, does not form any trihalomethanes (THMs) or halogenated organic compounds known to be carcinogenic. ClO_2 is an approved sanitizer for use as an aqueous solution on food-processing equipment and utensils at concentration at least 100 parts per million and not more than 200 parts per million available ClO_2 (FDA, 2019b). The main antimicrobial mechanism is due to oxidation of RNA, DNA, and proteins in the cell membranes allowing metabolic disruption (Sun, Baldwin, & Bai, 2019).

ClO_2 gas is more effective in reducing foodborne pathogens present in low numbers in inaccessible areas because ClO_2 gas has better penetration properties than the aqueous form (Han et al., 2001b). Additionally, gaseous sanitizers have been shown to have increased penetration capability and ability to reach inaccessible spots (Shynkaryk, Pyatkovskyy, Mohamed, Yousef, & Sudhir, 2015). The molecular size of the gas is known to be small (0.124 nm) (Arango, et al., 2014; Chai, Hwang, Huang, Wu, & Sheen, 2020; Lee, Burgess, Rubino, & Auras, 2015; Sun, Baldwin, & Bai, 2019; Sy, McWatters, & Beuchat, 2005).

ClO_2 gas is an excellent sanitizer for fresh fruits, vegetables, and equipment but has not been widely adopted. Few studies had been conducted to address the depletion/interaction of gas by materials that might be present during the decontamination procedure, such as organic matter (Arango, et al., 2014), aqueous films, and oil film (Hosni, Jang, Coughlin, & Bishop, 2006). Arango, *et al.* (2014) found that strawberries consume ClO_2 gas rapidily, and absoption of the gas went up to 45% of ClO_2.

In recent years, computational fluid dynamics (CFD) techniques are useful tools to understand and improve food processing. The commercial software COMSOL Multiphysics® 5.4 (COMSOL Inc., MA, USA) is a finite element methods-based software that can be used to develop multiphysics models to simulate decontamination procedure, used in food equipment. To date, there have been few studies applying CFD for modeling ClO_2 gas disinfection for food applications. The main objective of this study was to develop a physical-based model to analyze the

transport of ClO_2 involved in surface decontamination with and without water present. Therefore, it was needed to analyze the ClO_2 consumption by deionized water as a function of water volume, and surface area. In addition, these results were used to develop a mathematical model to simulate the gas diffusion during surface decontamination with chlorine dioxide.

2.3. Materials and methods

2.3.1. Schematic system - exposure chamber

The system (Figure 5) included a ClO_2 gas generator (Enerfab, Inc.; Cincinnati, OH), a 0.423 m^3 stainless steel reservoir, a 680 mL stainless steel exposure chamber, which contained a glass beaker used as a water reservoir; and a detection system that was able to monitor and record ClO_2 gas concentration in real-time. The experiment was run at room temperature (23 ± 2˚C), under dark conditions.

To generate ClO_2 gas, a mixture of [2%] Cl_2 gas and [98%] N_2, gas was pumped through a cartridge of sodium chlorite [74%], using a diaphragm pump. This reaction produced essentially pure ClO_2 gas at a concentration of 4%. The generated ClO_2 gas was injected into the stainless steel reservoir while an outlet valve remained open to avoid a pressure increase inside. The system was designed to achieve a target gas concentration of approximately 2500 ppm ± 100 ppm, where a human-machine interface EZ-S6M-R (EZAutomation, IA, USA) and a DL-06 programmable logic controller (AutomationDirect, Cumming, GA) was used to control a solenoid valve that allowed ClO_2 gas injection from the reservoir into the exposure chamber. This exposure chamber contained a glass chamber that held deionized water with different volumes. Three different diameters glass chambers (9.0397, 4.8125, and 1.6584 cm) were used to obtain varying surface areas (6.418, 1.819, and 0.216 $\times 10^{-3}$ m^2) for the same volumes of water.

The gas was pumped via a diaphragm pump through an Optek sensor Model AF26 (OPTEK Technology, Inc., TX, USA) and back to the chamber to measure concentration. Whenever the desired concentration was reached, all valves were closed to keep the gas circulating in the closed system (check dashed area in Figure 5). The detection system was equipped with an internal beam splitter making it possible to measure two wavelengths simultaneously. The Optek sensor measured concentration of ClO_2 gas based on the absorption of a dual-channel color sensor for two wavelength (385 and 550 nm) simultaneously. This sensor was connected to Optek Control 4000 photometric converted (OPTEK Technology, Inc., TX, USA), which determined the light absorption by the gas in real-time.

During the test, gas concentration was recorded continuously using a midi data logger GL240 (Graphtec America Inc., CA, USA) connected to the Optek Control 4000 to record voltage proportional to the signal from the sensor. This reading was directly related to the concentration of gas in the headspace of the exposure chamber. The data logger recorded the concentration in the exposure chamber until the concentration was below the detection limit of the sensor (300 ppm).

For the purpose of this study, ClO_2 concentration was expressed as ppm. The gas-phase concentration was recorded based on the following calibration curve:

$$\mathbf{y = 1130.5\,x - 812.4} \qquad (\mathbf{2.3.1})$$

where, x is the voltage (V) record by the midi data logger, and y is the ClO_2 gas concentration in ppm. The closed-loop simulated a scenario where a targeted quantity of ClO_2 gas was applied. This concentration in the gas phase depleted as the ClO_2 self-degraded, interacted with the walls of the vessel, or dissolved (or diffused) into deionized water over time.

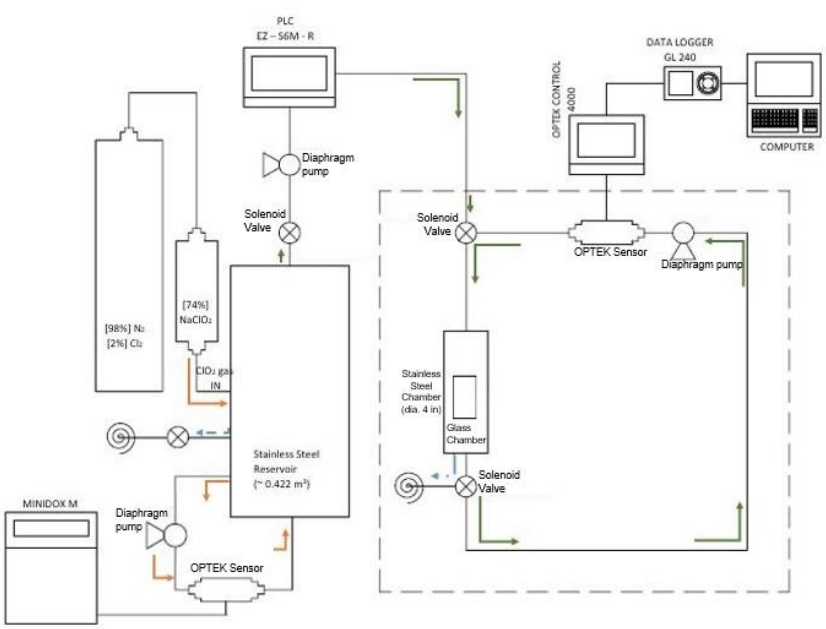

Figure 5. Schematic set up for chlorine dioxide depletion by deionized water. Dashed area shows the closed system that was monitored as gas concentration decayed over time.

2.3.2. Chlorine dioxide gas concentration decay over time

The decay of an initial concentration of ClO_2 gas as it interacted with other materials, species, or surfaces in the application environment, was explained with first-order exponential decay reaction kinetics. This was used to fit the control experiment (0 mL of water). This form included self-degradation, any possible reaction with stainless steel and glass walls, and any photodissociation due to the light used in the optical sensor. The equation for the first-order rate equation was:

$$\mathbf{A = A_0 e^{(-kt)}} \qquad (\mathbf{2.3.2})$$

where A is the concentration (ppm) over time, A_0 is the initial concentration, k is the slope of first-order reaction (1/s), and t is the time (s) that the reaction was monitored. The half-life ($t_{1/2}$) is the time required to reduce to half of its initial value and is independent of the starting concentration (equation 2.3.3).

$$t_{\frac{1}{2}} = \frac{\ln(2)}{k} \qquad (2.3.3)$$

Equations 2.3.4 and 2.3.5 explain how it was possible to fit the model with multiple first-order exponential terms, where a initial decay (k_1) was attributed to the addition of water compared in the chamber compared with the control experiment.

$$\mathbf{A = C_1 e^{(-k_1 t)} + C_2 e^{(-k_2 t)}} \qquad (2.3.4)$$

$$\mathrm{A_0} = \mathbf{C_1 + C_2}\ ; \mathrm{t} = 0 \qquad (2.3.5)$$

where, A is the concentration (ppm) over time, k_1 & k_2 are first-order reaction rates (1/s), and t is the time (s). Additionally, C_1 & C_2 are constants used to fit the reaction, where equation 2.3.5 shows that at t = 0, the sum of the two constants (C_1, C_2) are equal to the initial concentration (A_0). For this study, an initial concentration of 2500 ppm was injected into the exposure chamber where three different volumes of deionized water (20, 40, and 60 mL) were placed in the glass chamber, and three different surface areas were used for each volume (6.418, 1.819, and 0.216 $\times 10^{-3}$ m^2). The gas was monitored and recorded until the concentration dropped below the detection limit which ranged between 50 and 100 hrs. Then, curves of concentration depletion were compared.

2.3.3. Simulation model development: Geometric model

The computer simulation was developed using COMSOL Multiphysics ® 5.4 (COMSOL Inc., MA, USA) to simulate the transport of ClO_2 gas during surface decontamination. The transport of diluted species module in COMSOL was used in this study for simulating the diffusion of ClO_2. The diffusion coefficient was determined from the experiment conducted by Lee *et al.* (Lee, Burgess, Rubino, & Auras, 2015). This experiment explained the diffusion of ClO_2 gas from a reservoir to a collector through a diffusion tube (Figure 6), and was conducted under dark condition to minimize depletion due to photochemical dissociation.

The COMSOL model assumed gas application during surface decontamination was inside the equipment (dark condition). Therefore there was no photodissociation occur. The COMSOL model predicted the time for diffusion of ClO_2 gas to reach the bottom of a crevice in stainless steel equipment surfaces with the presence or absence of water on the crevice wall's. For each scenario simulated, the crevice varied in diameter and depth. The geometry of the model was designed to simulate the diffusion section of the Lee *et al.* (2015) experiment. Hence, two cylinder shapes were selected to simulate the diffusion tube and the collector vessel. Table 2 shows dimensions used for the two cylinders to simulate similar conditions to Lee *et al.* (2015) experiment. To increase the mesh quality and convergence rate, a finer size mesh was designed. Each cylinder was modeled using free tetrahedral elements and triangle elements where the average quality of each element was at least 0.8350 throughout the model.

2.3.4. Simulation model development: Governing equations

The model governing equations considering the mass transport of a gas within a crevice, can be assumed to be exclusively diffusive if no additional force is applied to ease the transport. The scenario can be stated as:

$$\frac{\partial c}{\partial t} + \nabla * (-D\nabla c) = -R \qquad (2.3.6)$$

where c is the concentration (mol/m^3), t is the time (s), D is the diffusion coefficient (m^2/s), and R (1/s) is associated with a first-order reaction rate, which for the model was considered the self-reaction reported by authors (Table 2). For the model development, the transport was assumed by diffusion only, with no reactions on the wall or surfaces, where n represents the unit normal vector, and the boundary condition was defined as:

$$\boldsymbol{n} * (D\nabla c) = 0 \qquad (2.3.7)$$

2.3.5. Simulation model development: Model validation

The model validation was conducted by comparing the predicted concentration of ClO_2 gas at the bottom of the collector vessel over time with the results shown by Lee*, et al. (2015)*. The model focused on the diffusion portion of the experiment and assumed that the initial concentration of 0.2179 mol/m^3 equivalent to 14.7 mg/L (5320 ppm) (Lee, Burgess, Rubino, & Auras, 2015) in the reservoir vessel was constant at the inlet of the diffusion tube for the mathematical simulation.

The transport of diluted species depends on the diffusion coefficient value which varies with temperature. The model focused on the effect of the diffusion coefficient on the final concentration at a point over time. Another, way to analyze the expected concentration at the collector vessel over time is through the following equations based on ClO_2 mass balance (Lee, Burgess, Rubino, & Auras, 2015; Pan & Zhu, 1998):

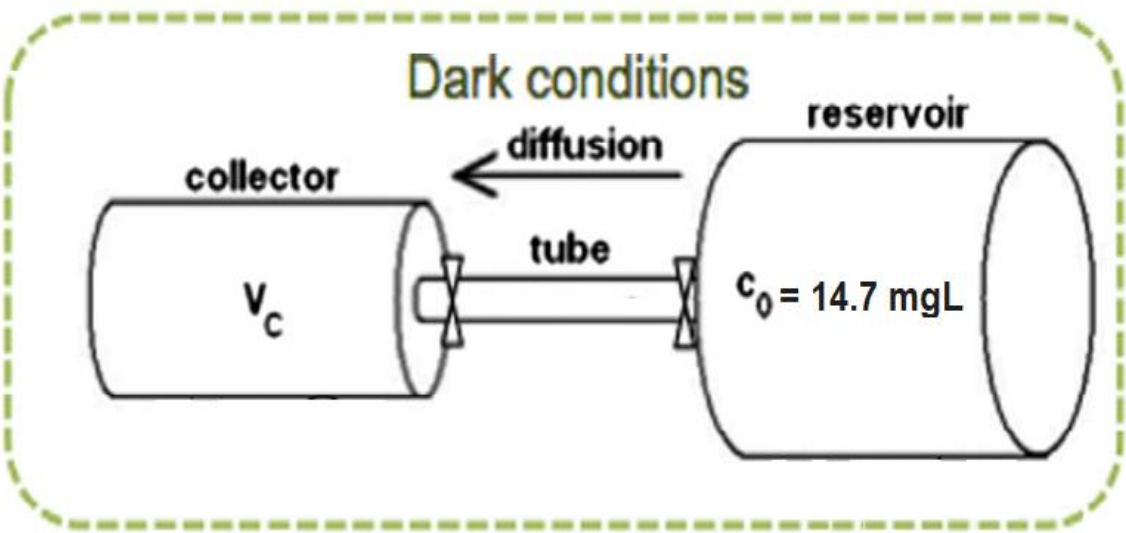

Figure 6. Chlorine dioxide gas diffusion from a reservoir to a collector through a diffusion tube. Adapted from (Lee, Burgess, Rubino, & Auras, 2015).

$$C_C(t) = \frac{C_0 \propto_C (e^{R_1 t} - e^{R_2 t}\}}{(R_1 - R_2)} \quad (2.3.8)$$

$$C_R(t) = C_0 \frac{\left(R_1 + k + \propto_c \cosh\left(L_{DT}\sqrt{\frac{k}{D}}\right)\right) e^{R_1 t} - \left(R_2 + k + \propto_C \cosh\left(L_{DT}\sqrt{\frac{k}{D}}\right)\right) e^{R_2 t}}{(R_1 - R_2)} \quad (2.3.9)$$

$$\propto_C = \frac{D\ A\sqrt{\frac{k}{D}}}{V_C \sinh\left(L_{DT}\sqrt{\frac{k}{D}}\right)} \quad (2.3.10)$$

$$\propto_R = \frac{D\ A\sqrt{\frac{k}{D}}}{V_R \sinh\left(L_{DT}\sqrt{\frac{k}{D}}\right)} \quad (2.3.11)$$

where, C_R (mol/m^3) is the concentration at the reservoir, and C_C (mol/m^3) is the concentration at the collector. Both concentrations were analyzed over t, which is time (s). V_C is the volume of the collector vessel (m^3), V_R is the volume of the reservoir vessel (m^3), A is the cross-sectional area of the tube (m^2). C_0 (mg/L) at is the initial concentration of the system; L_{DT} is the length of the diffusion tube (0.10 m), k is the reaction rate (1/s), and D is the diffusion coefficient (m^2/s). Additionally, R_1 and R_2 are the roots of the quadratic equation 2.3.12:

$$R^2 + \left[2k + (\propto_C + \propto_R)\cosh\left(L\sqrt{\frac{k}{D}}\right)\right]R + \left[k^2 + k(\propto_C + \propto_R)\cosh\left(L\sqrt{\frac{k}{D}}\right) - \propto_C \propto_R\ sinh^2\left(L\sqrt{\frac{k}{D}}\right)\right] = 0 \quad (2.3.12)$$

The diffusion coefficient D was fitted to the experimental results reported by the authors by minimizing the sum of the squares of the errors between the concentrations over time predicted with the equation 2.3.8, and the experiments from previous research (Lee, Burgess, Rubino, & Auras, 2015). Table 2 shows the values used for each parameter in equation 2.3.8 during calculations.

2.3.6. Simulation model development: Simulation model of ClO_2 gas diffusion in air into crevices

Once a mathematical model was developed and validated, it was used to predict the time needed for the desired concentration of ClO_2 gas to reach the bottom of a crevice in stainless steel equipment. Additionally, the reaction value due to water obtained from previous experiments was incorporated into the mode by adding a surface reaction term. This addition to the model should account for surface decontamination scenarios were a film of water may be present inside the crevice walls.

Table 2 shows the parameters used to develop the mathematical model. For any scenario, the diffusion occurred into two different crevice diameters (1 and 5 mm). Additionally, the simulation was run for three different crevice depths (1mm, 10 mm, and 100 mm). Since the simulation assumed that the decontamination procedure occurred under dark conditions, and the temperature was kept at 23 °C, the ClO_2 gas diffusion coefficient for the model was 0.145 cm^2/s (Lee, Burgess, Rubino, & Auras, 2015), and 0.160 cm^2/s based on the theory of diffusion in gases at low density (Bird, Stewart, & Lightfoot, 2006).

2.3.7. Statistical analysis

The effects of volume of water and exposure surface area on the slopes of reaction, and half-time were analyzed using one-way repeated ANOVA. Diagnostic analysis was conducted to exam model assumptions for normality and equal variance. Post hoc multiple comparisons were performed with Tukey's adjustment. Statistical significance was identified at the level of 0.05. Analyses were conducted in SAS 9.4 TS1M4 for Windows 64x (SAS institute Inc., Cary, NC).

2.4. Results and discussion

2.4.1. Chlorine dioxide gas concentration decay over time

The decay of ClO_2 gas concentration inside a closed chamber with three different volumes of deionized water (20, 40, and 60 mL), and 0 mL (control) was monitored for each surface area (6.418, 1.819, and 0.216 $\times 10^{-3}$ m^2). For the control, the decay over time was fitted into a first-order rate (Figure 7 & Figure 8). Where the gas concentration reduced by half after 27.52 h. This decay could be due to photodissociation by the optical sensor light, reaction with inner walls, and self-degradation (Lee, Burgess, Rubino, & Auras, 2015).

Table 2. Experimental parameters for the chlorine dioxide gas diffusion used in the model

Parameters	Value
Initial concentration[1]	C_0 = 14.7 mg/L (0.2179 mol/m^3)
Diameter of diffusion tube[1]	$ø_{DT}$ = 4.76 mm
Length of diffusion tube[1]	L_{DT} = 100 mm
Volume of diffusion tube	V_{DT} = 1179.52 mm^3
Diameter of collector vessel	$ø_C$ = 35.7 mm
Length of collector vessel	L_C = 100 mm
Volume of collector vessel[1]	V_C = 400 mL (4x10^{-4} m^3)
Volume of reservoir vessel[1]	V_R = 2200 mL (2.20 x10^{-3} m^3)
Diffusion coefficient of ClO_2 (23 °C)[1]	D = 1.45x10^{-5} m^2/s (0.145 cm^2/s)
Diffusion coefficient of ClO_2 (23 °C)[2]	D = 1.60x10^{-5} m^2/s (0.160 cm^2/s)
Volume first-order reaction (k) of ClO_2 (23°C) - Self-reaction[1]	k = 7.007 x10^{-5} 1/min (1.17x10^{-7} 1/s)
α_c	3.04 x10^{-4} 1/min
α_R	5.53 x10^{-5} 1/min
R_1	- 7.00 x10^{-5} 1/min
R_2	- 4.30 x10^{-4} 1/min
Surface first-order reaction (k) of ClO_2 (23°C) - Wall reaction	6.8378 1/h *from Section 2.4.4*
Diameters of crevices	dia. 1 mm dia. 5 mm
Length of crevices	Len. 1 mm Len. 10 mm Len. 100 mm

Note: [1] - Values obtained from (Lee, Burgess, Rubino, & Auras, 2015)
Note: [2] - Values obtained from (Bird, Stewart, & Lightfoot, 2006)

Between different first-order reaction chemical kinetics curves with similar conditions, different values for reaction rate (k) explained the difference mentioned above. For the control, the reaction rate was estimated to be 7.03×10^{-6} s^{-1} at any exposure surface area, which is significantly higher than the reaction rate reported by previous researchers under similar conditions, e.g. 1.17×10^{-6} s^{-1} (Lee, Burgess, Rubino, & Auras, 2015) and 0.38×10^{-6} s^{-1} (Arango, et al., 2014). This difference may be explained by to the material of the chamber. In the experiments conducted by (Lee, Burgess, Rubino, & Auras, 2015) and (Arango, et al., 2014), the chambers were made of glass, whereas the chamber used here was stainless steel AISI316 and AISI304. These materials likely increased the reaction with the walls, and created minor corrosion in the inner walls of the chambers.

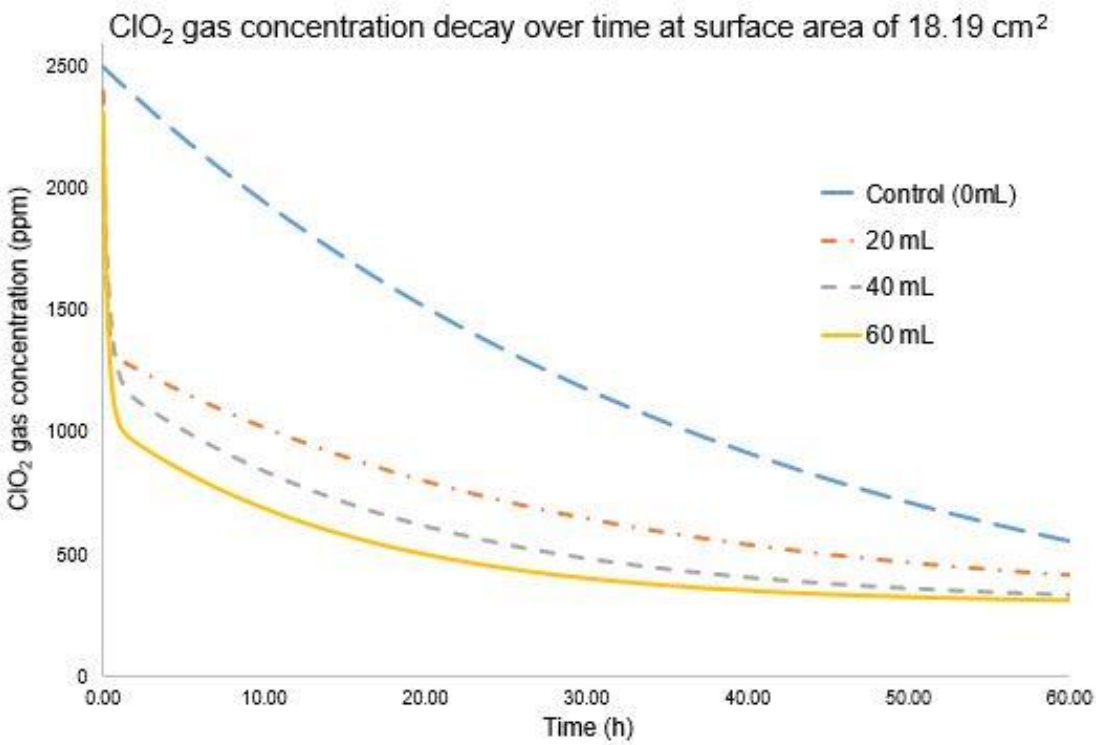

Figure 7. Chlorine dioxide concentration versus time for control and different volume of deionized water at surface area of 1.819×10^{-3} m^2. Values fitted of first-order reaction equations 2.3.2 (for control) and 2.3.4 for 20, 40 and 60 ml.

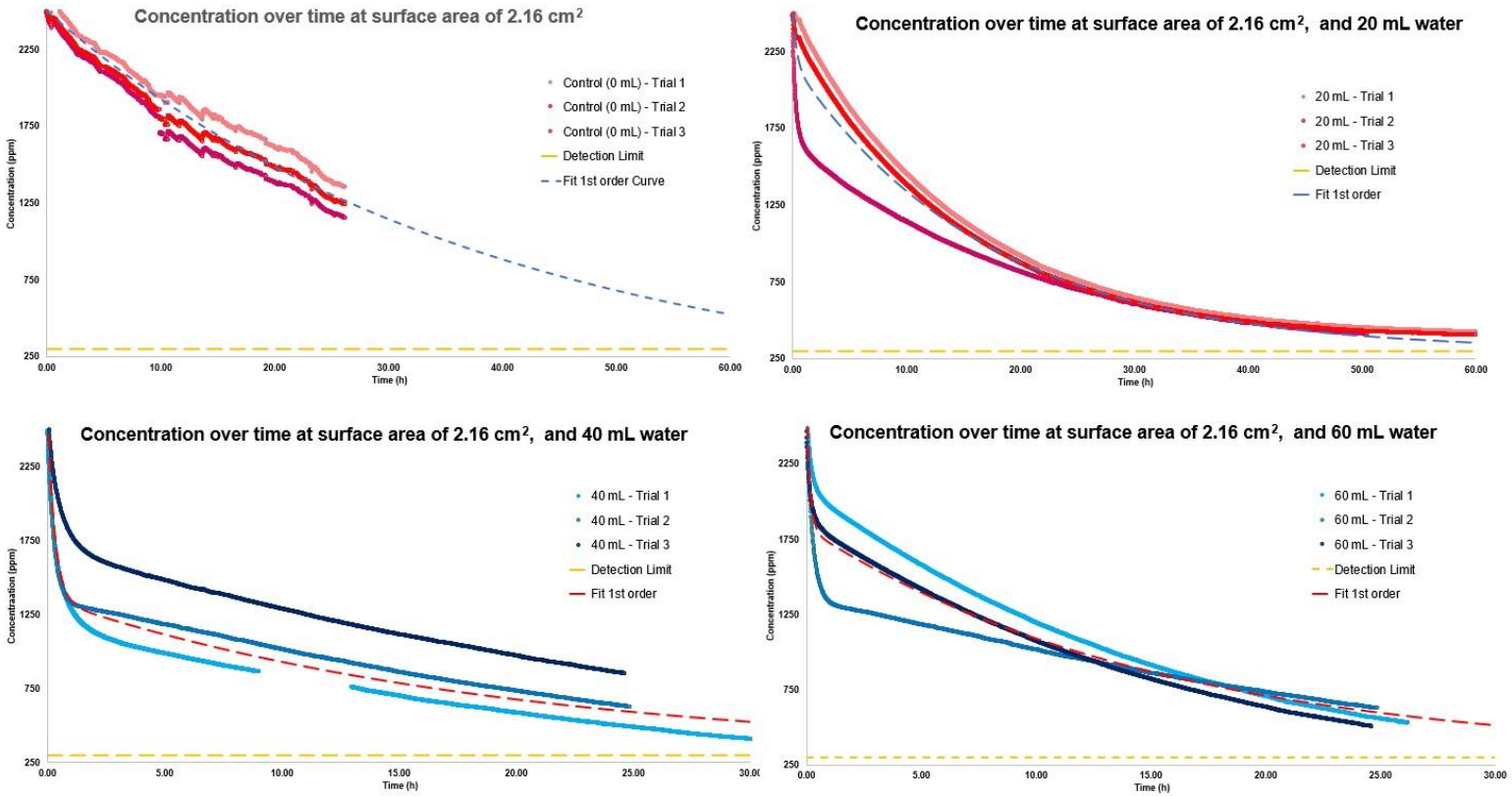

Figure 8. Raw data fitted to the two-term exponential decay of ClO_2 gas concentration over time for varying water volumes at a constant surface areaa of 2.16, 18.19, and 64.18 cm^2

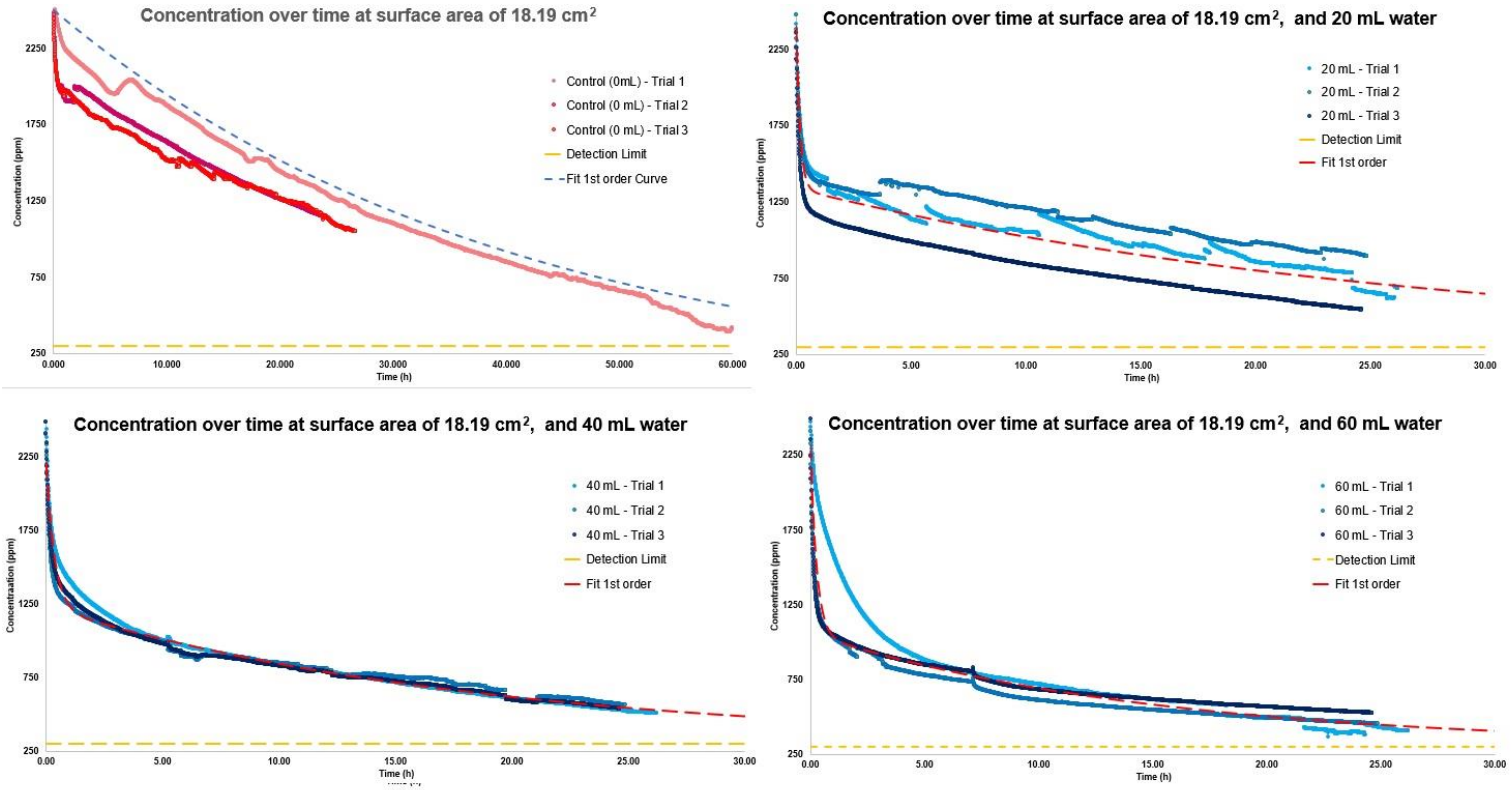

Figure 8. Continued

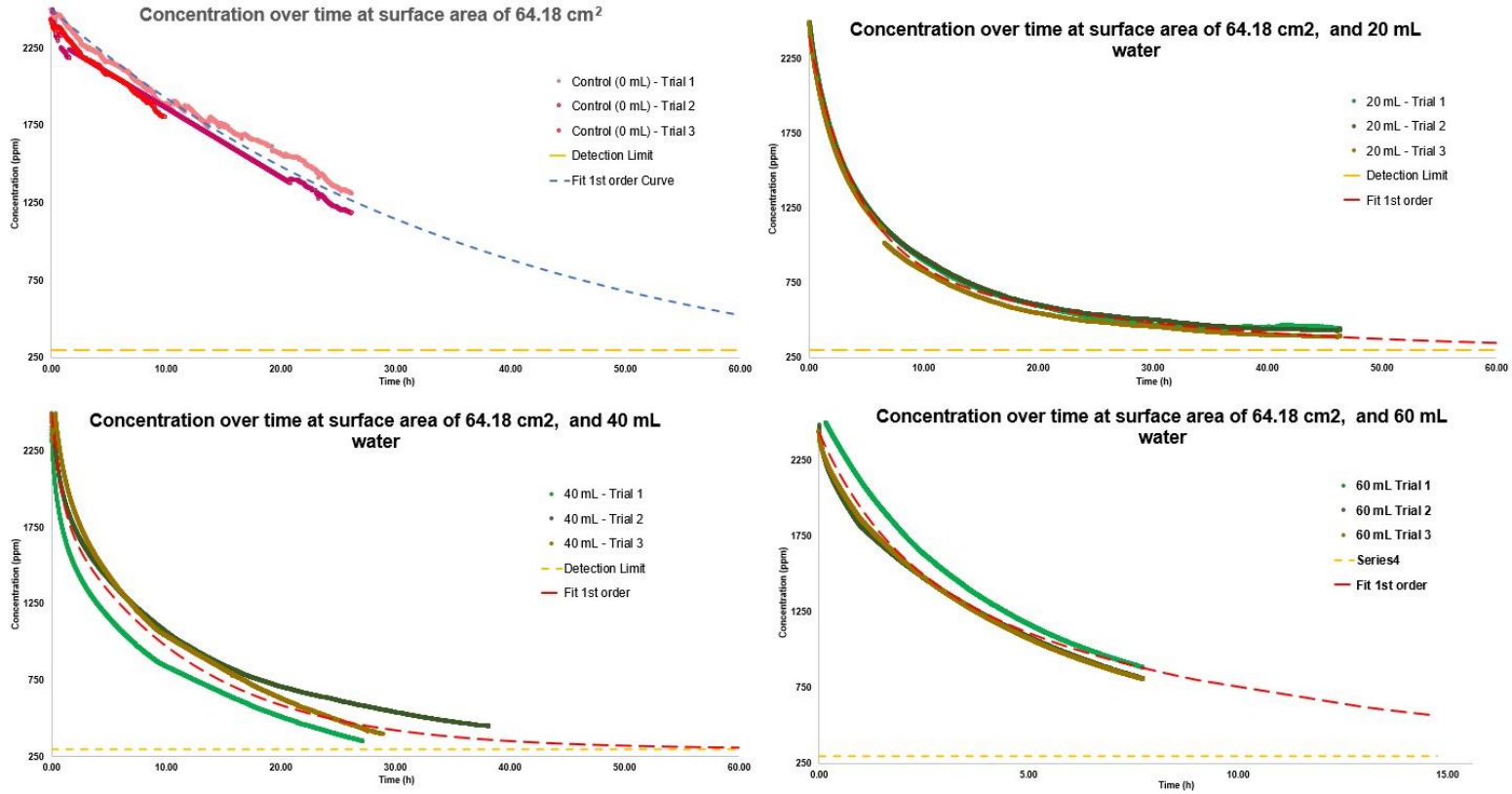

Figure 8. Continued

Table 3. First-order reaction rate k_1 [1/h] of ClO_2 gas at different volume of deionized water and different exposure surface area

Deionized water volume	Exposure surface area		
	64.18 cm^2	**18.19 cm^2**	**2.16 cm^2**
Control (0 mL)	0.026 ± 0.003 (A-b)	0.025 ± 0.002 (A-b)	0.025 ± 0.003 (A-c)
20 mL	0.253 ± 0.019 (C-b)	6.021 ± 1.587 (A-a)	2.911 ± 0.474 (B-bc)
40 mL	1.206 ± 0.646 (A-a)	2.791 ± 1.188 (A-ab)	3.333 ± 1.375 (A-b)
60 mL	0.595 ± 0.101 (B-ab)	3.720 ± 2.535 (AB-ab)	6.838 ± 1.990 (Aa)

Values are reported as average ± standard deviation (n = 3)
Note: a-b. Different letters indicate significant difference among data in the colums ($p < 0.05$)
Note: A-B. Different letters indicate significant difference among data in the row ($p < 0.05$)

The gas decay over time due to water present was fit to a first-order exponential decay with two reaction rates (k_1 and k_2), following equation 2.3.4.. Table 3 shows k_1 of the gas for 20, 40, and 60 mL of deionized water in the exposure chamber was approximately 2.911, 3.333, and 6.838 1/h, respectively, at 0.216 $\times 10^{-3}$ m^2 water surface area. Whereas, k_1 was 6.021, 2.791, and 3.720 1/h, respectively, at 1.819 $\times 10^{-3}$ m^2 water surface area. Finally, the k_1 was 0.253, 1.206, and 0.595 1/h respectively, at 6.418 $\times 10^{-3}$ m^2 water surface area. The first-order reaction rate was significantly higher whenever the chamber included water, at each exposure surface area. This difference was attributed to the dissolution of the ClO_2 gas into the water since the aqueous phase was not detected by the optical sensor. This implied a faster reduction of ClO_2 gas in the air due to the presence of deionized water. No significant correlation was found both a higher volume of water and a larger water surface area exposed to the gas.

Furthermore, at different deionized water volume 20, 40, and 60 mL at exposure surface area of 0.216 $\times 10^{-3}$ m^2, the second reaction rate (k_2) was estimated to be 0.059, 0.051, and 0.066 1/h, respectively. At an exposure surface area of 1.819$\times 10^{-3}$ m^2, k_2 was estimated to be 0.036, 0.054, 0.066 1/h, respectively. Finally, at an exposure surface area of 6.418 $\times 10^{-3}$ m^2, the reaction rate k_2 was estimated to be 0.045, 0.085, 0.109 1/h, respectively (Table 4). Overall, the values for k_1 indicated a faster decay for the ClO_2 gas in the headspace than for k_2 for each water volume and surface area. A previous study showed that ClO_2 gas is also consumed by strawberry in a closed chamber. That research showed an increment in the reaction rate from 0.38$\times 10^{-6}$ s^{-1} to 9.78$\times 10^{-6}$ s^{-1}, when 1 kg of strawberry was exposed to 1 mg/L in an 11 L custom-built glass chamber (Arango, et al., 2014). Similarly, this experiment showed that water in the system increases the reaction rate.

Table 4. First-order reaction rate k_2 [1/h] of ClO_2 gas at different volume of deionized water and different exposure surface area.

Deionized Water Volume	Exposure surface area		
	64.18 cm^2	**18.19 cm^2**	**2.16 cm^2**
Control (0mL)	0.026 ± 0.003 (A-b)	0.025 ± 0.002 (A-c)	0.025 ± 0.003 (A-b)
20 mL	0.045 ± 0.004 (AB-b)	0.036 ± 0.012 (B-bc)	0.059 ± 0.009 (A-a)
40 mL	0.085 ± 0.021 (A-a)	0.054 ± 0.005 (A-ab)	0.051 ± 0.013 (A-ab)
60 mL	0.109 ± 0.014 (A-a)	0.066 ± 0.010 (B-a)	0.066 ± 0.017 (B-a)

Values are reported as average ± standard deviation (n = 3)
Note: The control experiment only include k_1
Note: a-b. Different letters indicate significant difference among data in the column ($p < 0.05$)
Note: A-B. Different letters indicate significant difference among data in the row ($p < 0.05$)

The first reaction rate (k_1) was attributed to the ClO_2 gas getting into the water, while the second reaction rate (k_2) was attributed to the self-degradation, photodissociation, and ClO_2 gas reaction with inner walls. To keep a certain concentration, while reaching equilibrium, in a larger amount of water requires a higher amount of dissolved ClO_2 (Gates, 1998; Sander, 2015). Additionally, figure 7 shows a larger exposure surface area for the water in contact with the gas increased the overall decay rate for a surface area of 1.819×10^{-3} m^2.

A measurement of the ClO_2 gas in water was made using the DPD-glycerol method, where the aqueous concentration was determined after the concentration in the headspace reached below the detection level (300 ppm). The values found were 2.49, 4.96, and 5.28 mg/L at the aqueous phase, for 20, 40, and 60 mL of deionized water in the system at an exposure surface area of 1.819×10^{-3} m^2, respectively. The concentration in the headspace was below 0.82 mg/L (detection level). The aqueous phase was found to be at least 3.03, 6.05, and 6.44 times greater than the headspace. This demonstrated that ClO_2 does not dissolve in the water as gas, but it might reduced to ionic form chlorite (ClO_2^{-1}), chlorate (ClO_3^{-1}), and chloride (chlorite (Cl^{-1}).

According to Henry's Law, the concentration in the aqueous phase should be around 23 times higher than the gaseous phase. This difference seen at the end of our experiments was attributed to the decreasing gas concentration in the headspace where the system was not in equilibrium (Gates, 1998; Sander, 2015). Also, the measurement of ClO_2 concentration in the aqueous phase was done after the headspace was below the detection level. This means that most of the ClO_2 had converted to one of the forms mentioned above. Further studies should focus on quantifying the fate of the ClO_2 in the water.

2.4.2. Simulation model validation

The initial model was developed to simulate the diffusion of ClO_2 in air by validating with results found in previous research (Lee, Burgess, Rubino, & Auras, 2015). In that study, reservoir and collector vessels were connected by a diffusion tube. In this model, just the diffusion through the tube to the collector vessel was considered. Two cylinders were used to model the tube (dia. 4.76 mm, and length 100mm) and the collector vessel (dia. 3.57 cm, and length 10 cm). In this study, the simulation assumed a constant concentration of 14.7 mg/L at the inlet of the diffusion tube as the gas diffused to the collector vessel. The geometry was discretized into a mesh, which (Figure 9) consisted of about 23,204 tetrahedral elements and 5214 triangles with 0.5525 of minimum element quantity calculated by COMSOL Multiphysics® 5.4.

For the validation of the simulated transport of ClO_2 gas over time, the average concentration in the collector was compared with the experimental concentration reported by the authors (Lee, Burgess, Rubino, & Auras, 2015). Additionally, the simulation was compared to the predicted concentrations over time at the collector by using the equation (2.3.8) based on the mass balance of ClO_2 (Lee, *et al*., 2015).

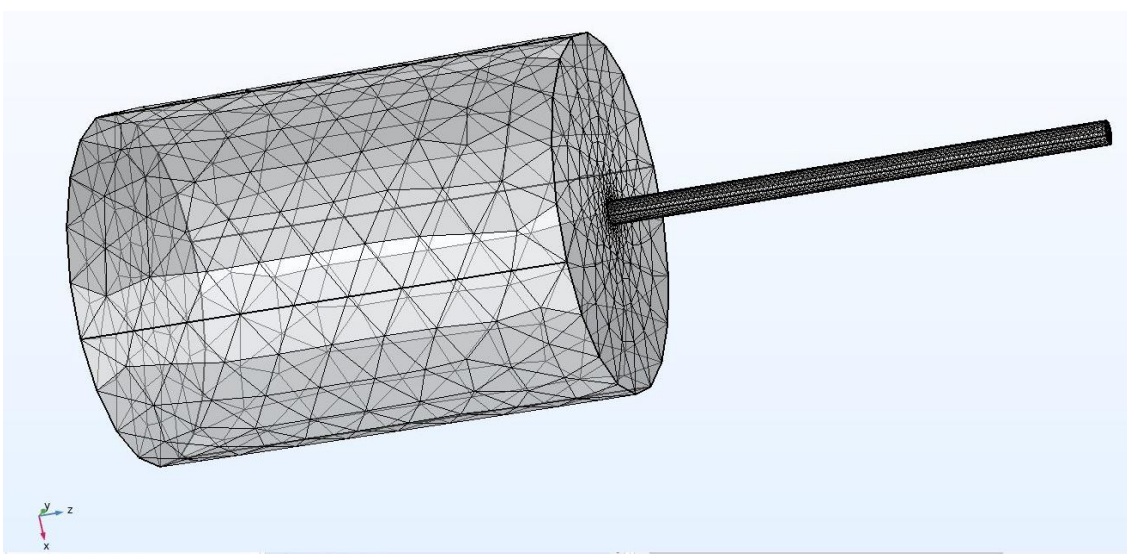

Figure 9. Meshing scheme of the diffusion tube and collector vessel.

The simulation prediction by the COMSOL software and the prediction by equation 2.3.8 from the mass balance are shown in Figure 10. The prediction by the software and the equation are similar. The blue lines show the predicted values using the diffusion coefficient from the theory of diffusion in gases at low density 0.160 cm^2/s (Bird, Stewart, & Lightfoot, 2006). The dashed blue line shows the predicted values from the analytical equation, and the solid blue line shows the values from the COMSOL simulation. At time 0 min, 10, 30, 60, 180, 360, and 720 min the concentration of ClO_2 gas at the collector for the simulation by the software was 0.000, 0.050, 0.172, 0.351, 1.039, 1.998, and 3.707 mg/L, respectively. Meanwhile, at the same time the concentration for the prediction by equation 2.3.8 was 0.000, 0.063, 0.187, 0.370, 1.072, 2.020, and 3.614 mg/L, respectively.

The red lines show the predicted values whenever the diffusion coefficient of the gas was assumed to be 0.145 cm^2/s based on the coefficient of diffusion reported by the authors at 23°C. Similarly, the solid red line shows the predicted values by the simulation at times of 0, 10, 30, 60, 180, 360, and 720 min where the concentration at the collector vessel was 0.000, 0.045, 0.155, 0.318, 0.944, 1.824, and 3.405 mg/L, respectively. Additionally, the dashed line shows the predicted values from the equation, which at times of 0 min, 10, 30, 60, 180, 360, and 720 min, the concentration at the collector vessel was 0.000, 0.057, 0.169, 0.336, 0.976, 1.846, and 3.329 mg/L, respectively.

It was shown that the concentration over time at the collector vessel by the COMSOL simulation and the mathematical equation were similar. Both values were compared with the observed concentration at the collector as measured by the authors (Lee, Burgess, Rubino, & Auras, 2015). Despite, the simulation predictions being similar to values predicted from equation 2.3.8, both values were not close to the values measured by the authors (Figure 10). This discrepancy could be due to measurement, due to reaction with inner walls, or photo dissociation by the UV detector during the experiments (Davis & Lee, 1996; Lee, Burgess, Rubino, & Auras, 2015). Any of these factors could explain the reason why the observed concentration at the collector reported by the authors was lower than the predicted values by simulation, and the mass balance equation.

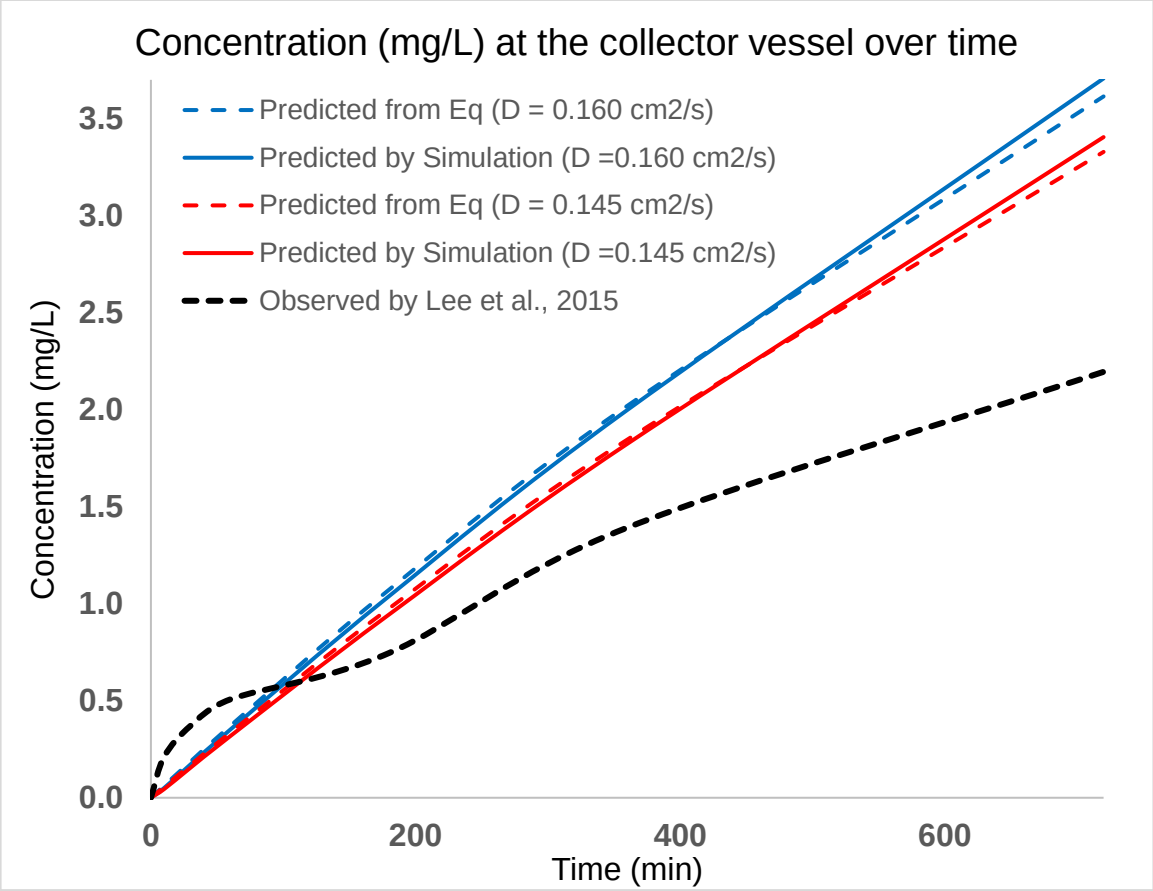

Note: Blue lines show the prediction using a diffusion value D=0.160 cm^2/s. Red lines show the prediction using D=0.145 cm^2/s

Figure 10. Comparison between predicted values (Equation 2.3.8 & COMSOL simulation) and observed values of ClO_2 concentration (mg/L) at the collector vessel during diffusion through 4.76 mm x 100mm tube with different diffusion coefficients.

The diffusion coefficient value reported by Lee*, et al.* (2015) (0.145 cm^2/s) was selected to be the best fit to the experimental data (Lee, Burgess, Rubino, & Auras, 2015) while minimizing the sum of squares of errors between the predicted concentration from equation 2.3.8 and 2.3.9, and the measured concentrations by adjusting the diffusion coefficient. However, the same calculation was performed in this study, and the best fit diffusion coefficient was 0.097 cm^2/s. This lower coefficient was better able to predict the values observed by authors (Figure 11). The concentrations predicted by the simulation using a diffusion coefficient of 0.097 cm^2/s at 0, 10, 30, 60, 180, 360, and 720 minutes were 0.000, 0.026, 0.100, 0.210, 0.637, 1.248, and 2.378 mg/L, meanwhile, the observed values at those same time period were 0.000, 0.211, 0.371, 0.507, 0.746, 1.392, and 2.195 mg/L, respectively.

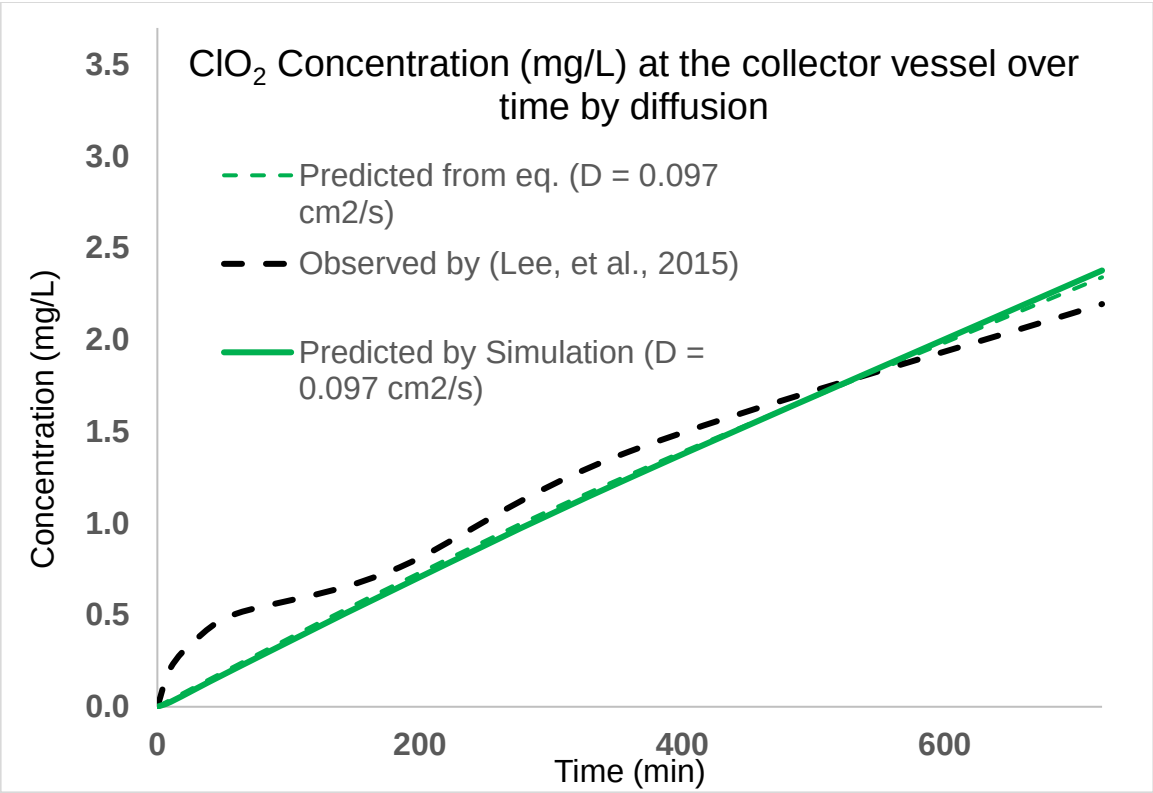

Note: Green lines showed the prediction using a diffusion value of 0.097 cm^2/s

Figure 11. Comparison between predicted values (Equation 2.3.8 & COMSOL simulation) and observed values of ClO_2 concentration (mg/L) at the collector vessel during diffusion through 4.76 mm x 100mm tube

2.4.3. Simulation model ClO_2 gas diffusion in the air into crevices

Based on the comparison between the physics-based model, and the experimental results observed by the authors, the diffusion coefficient of 0.097 cm^2/s was used to evaluate the diffusion of the gas during surface decontamination because it minimized the sum of square of the errors. The diffusion coefficient of 0.145 cm^2/s was also used because it was reported by the authors (Lee, Burgess, Rubino, & Auras, 2015). For both models, the initial concentration for ClO_2 gas was selected as 1 mg/L, and assumed to be constant during the decontamination procedure. The simulation solved for the time needed for the gas to reach the bottom of two cylindrical crevices with combinations of diameter (1 mm & 5 mm) and depth (1 mm, 10mm & 100 mm).

Table 5, shows the time needed for the bottom of the crevice to reach the initial ClO_2 gas concentration using the diffusion coefficient of 0.145 cm^2/s. Table 4

shows three possible crevice situations with fixed diameters of 1 mm and 5 mm and three depths for each: 1 mm, 10 mm, and 100 mm. The physics-based model correctly shows that the time needed for the ClO_2 to reach the bottom is depth-dependent considering the same diffusion coefficient. The time to reach the concentration of 1 mg/L at the bottom of crevices 1, 10, and 100 mm depth was 0.15, 15, and 1700 seconds, respectively. This physics-based model was similar to the one shown in previous research (Shynkaryk, Pyatkovskyy, Mohamed, Yousef, & Sudhir, 2015) where the authors simulated gaseous ozone instead of ClO_2 for the same three depths 1, 10, and 100 mm and a channel of 1 mm wide. The time required for the ozone gas to reach equilibrium in the channel was 0.10, 10, and 1000 seconds, respectively. The authors reported a diffusion coefficient of the ozone gas of 0.147 cm^2/s, suggesting a slightly faster transport of the ozone molecule than ClO_2, which was noticed in the time needed at similar conditions. The difference between the diffusion coefficient might be due to the molecular weight since ozone molecules have a smaller molecular weight (48.00 g/mol) than ClO_2 (67.45 g/mol), and based on the theory of the low density gas, lighter molecules are predicted to have a higher diffusion coefficient (Bird, *et al.*, 2006).

Additionally, Table 6 shows the time needed for the bottom of a 1 mm & 5 mm diameter crevice to reach the initial ClO_2 gas concentration using the diffusion coefficient of 0.097 cm^2/s. Similarly, the time was depth-depent and both diameters showed similar times for the gas to reach the bottom. Table 6 shows the time needed was 0.22, 22, and 2700 seconds, respectively.

The time needed for the bottom of the crevice to reach the initial concentration of ClO_2 gas within the same scenarios is directly related to the value of the diffusion coefficient. The ClO_2 gas diffusion coefficient value of 0.145 cm^2/s based on the experiments by previous authors (Lee, Burgess, Rubino, & Auras, 2015), is about 50% greater than the value of 0.097 cm^2/s. This gas movement is typically explained by Fick´s first law where a greater diffusion coefficient yields a shorter time to reach a certain concentration (Bird, Stewart, & Lightfoot, 2006). The difference in time needed for the bottom of the crevices to reach the initial ClO_2 gas concentration was found to be about 46% faster at diffusion coefficient value of 0.145 cm^2/s than the value of 0. 097 cm^2/s

The simulation showed that crevice depth should be considered whenever chlorine dioxide gas is used as a sanitizer during the decontamination of equipment. The simulation is sensitive to the diffusion coefficient of the gas in air, so an accurate value of the gas diffusion coefficient is critical to estimate time to reach the desired concentration in any crevices. The desired concentration was reached at the bottom of the crevice almost instantly whenever the depth was 1 mm, despite the diffusion coefficient used. Additionally, when the depth was 10 mm, the time needed for the gas to reach the bottom of the crevice was 15 seconds at a diffusion coefficient value of 0.145 cm^2/s and 22 seconds at 0.097 cm^2/s. Typically, ClO_2

gas is used as a sanitizer to inactive pathogens on food contact surfaces. Applications are highly varied according to the food surfaces, target microorganism, temperature, and relative humidity during treatment. However, typical contact times for various applications are between seconds to minutes (Sun, Baldwin, & Bai, 2019). This means that some crevices in equipment could impact the effectiveness of the ClO_2 gas treatment due to the time for gas to diffuse into the crevice in order to be effective at killing microorganisms.

2.4.4. Simulation model ClO_2 gas diffusion in the air into crevices with water present

Since many crevices in equipment and food surfaces may not be completely dry, the model was modified to include the reaction rate of ClO_2 in the presence of water obtained from the previous results (Table 4). Again, a constant concentration for ClO_2 gas of 1 mg/L in the inlet of the crevice was used during the decontamination procedure. The worst-case scenario with a reaction rate of 6.8378 1/h was selected. Further analysis was done where scenarios assumed the diffusion coefficients of 0.097 cm^2/s and 0.145 cm^2/s.

The model simulated the concentration at the bottom of the crevices. Table 7 shows the time needed for the gas to reach the bottom of crevices (with combinations of diameters of 1 and 5 mm and depths of 1, 10, and 100 mm) with water present in the inner walls. This model shows the impact of surface water in the crevice on the time for the gas to reach the bottom of the crevice. Using a diffusion coefficient of 0.145 cm^2/s, the time to reach a concentration of 1 mg/L at the bottom of a crevice with depth of 1 mm and 10 mm was 0.15 and 15 seconds, respectively, which was similar at both diameters. However, after 10000 seconds the bottom of the 100 mm crevice did not reach beyond 0.57 mg/L. Table 8 shows the time needed for the ClO_2 gas to reach the bottom of a 1 mm and 5 mm diameter crevice using a diffusion coefficient of 0.097 cm^2/s. Similarly, the time needed for the ClO_2 gas to reach the initial concentration at 1 mm and 10 mm depths was 0.22 and 22 seconds, respectively. Nonetheless, after 10000 seconds the concentration of the bottom of the 100 mm deep crevice (diameter of 1 and 5mm) did not reach beyond than 0.45 mg/L.

Overall, the presence of water on the inner wall of a crevice did not change the time for diffusion significantly compared to a dry crevice, at depth of 1 mm and 10 mm. This is due to the small exposure surface area in the crevice, as well as the small volume of water. The water was assumed to be on the walls of the crevice. As shown in Table 4, the ClO_2 gas concentration is surface area- and water volume-dependent. Since the small surface area and low water volume was present on the surface of the crevice, the difference in time with and without water

present was insignificant. However, a depth of 100 mm impacted significantly the concentration reached at the bottom

2.5. Conclusions

The goal of this chapter was to develop a physical-based model to analyze the time needed for ClO_2 gas to transport to the bottom of crevices involved in surface equipment decontamination. To fulfilled it, it was neccesaty to determine the reaction rate of ClO_2 gas due to the exposure to water at different surface areas and water volumes, also it was needed to evaluate the effect of diffusion coefficient. Finally, these generated data were incorporated into the model to evaluate the ClO_2 diffusion process.

The reaction rate of the ClO_2 gas increased with water present. Additionally, a COMSOL model was developed to simulate the ClO_2 gas transport inside a crevice during surface decontamination. The research aimed to provide information and a model that could be used for engineering design purposes to predict the gas treatment time needed to achieve adequate surface decontamination with crevices present in the surface.

In conclusion, the experiment suggested that the ClO_2 gas concentration decayed after reacting with the stainless steel chamber, as well as it dissolved into water. The simulation showed that depth of the crevice is an important factor to be considered and showed that the gas was efficient to transport to a depth of 1 mm and 10 mm. The time for gas transport into small crevices is more affected by diffusion coefficient than water reaction rate. Therefore, an accurate estimate of gas diffusion coefficient is most important when predicting the time for gas to reach the bottom of crevices.

To expand the research, different concentrations of ClO_2 gas, and exposure durations are needed to address the impact in the reaction rate with water. Further research can also be extended to determine the rate of ClO_2 molecules dissolving into water, and the residuals form. This information is needed to improve the model application and accuracy.

.

Table 5. Average concentration (mg/L) at the bottom of the crevice over time. Using a diffusion coefficient of 0.145 cm^2/s

Time (s)	Depth = 1 mm		Time (s)	Depth = 10 mm		Time (s)	Depth = 100 mm	
	dia. 1 mm	dia. 5 mm		dia. 1 mm	dia. 5 mm		dia. 1 mm	dia. 5 mm
0.00	0.00	0.00	0.00	0.00	0.00	0.00	0.00	0.00
0.01	0.13	0.14	1.00	0.13	0.13	1.00	0.00	0.00
0.02	0.38	0.39	2.00	0.38	0.38	5.00	0.00	0.00
0.03	0.57	0.58	3.00	0.57	0.57	10.00	0.00	0.00
0.04	0.70	0.71	4.00	0.70	0.70	100.00	0.13	0.13
0.05	0.79	0.80	5.00	0.79	0.79	500.00	0.79	0.79
0.06	0.86	0.86	6.00	0.85	0.85	600.00	0.85	0.85
0.07	0.90	0.90	7.00	0.90	0.90	800.00	0.93	0.93
0.08	0.93	0.93	8.00	0.93	0.93	900.00	0.95	0.95
0.09	0.95	0.96	9.00	0.95	0.95	1000.00	0.97	0.97
0.10	0.97	0.97	10.00	0.97	0.97	1100.00	0.98	0.98
0.11	0.98	0.98	11.00	0.98	0.98	1200.00	0.98	0.98
0.12	0.99	0.99	12.00	0.99	0.98	1300.00	0.99	0.99
0.13	0.99	0.99	13.00	0.99	0.99	1400.00	0.99	0.99
0.14	0.99	0.99	14.00	0.99	0.99	1500.00	0.99	0.99
0.15	1.00	1.00	15.00	1.00	1.00	1600.00	0.99	1.00
0.16	1.00	1.00	16.00	1.00	1.00	1700.00	1.00	1.00
0.17	1.00	1.00	17.00	1.00	1.00	1800.00	1.00	1.00
0.18	1.00	1.00	18.00	1.00	1.00	1900.00	1.00	1.00
0.19	1.00	1.00	19.00	1.00	1.00	2000.00	1.00	1.00
0.20	1.00	1.00	20.00	1.00	1.00	2100.00	1.00	1.00

Table 6. Average concentration (mg/L) at the bottom of the crevice over time. Using a diffusion coefficient of 0.097 cm^2/s

Time (s)	Length = 1 mm		Time (s)	Length = 10 mm		Time (s)	Length = 100 mm	
	dia. 1 mm	dia. 5 mm		dia. 1 mm	dia. 5 mm		dia. 1 mm	dia. 5 mm
0.00	0.00	0.00	0.00	0.00	0.00	0.00	0.00	0.00
0.01	0.04	0.05	1.00	0.04	0.05	100.00	0.05	0.05
0.02	0.21	0.23	2.00	0.22	0.22	200.00	0.21	0.22
0.04	0.51	0.53	4.00	0.51	0.51	400.00	0.50	0.51
0.05	0.61	0.63	5.00	0.60	0.62	500.00	0.61	0.62
0.10	0.89	0.89	10.00	0.90	0.89	1000.00	0.90	0.89
0.11	0.91	0.92	11.00	0.91	0.91	1100.00	0.91	0.91
0.12	0.93	0.93	12.00	0.95	0.93	1200.00	0.95	0.95
0.13	0.95	0.95	13.00	0.97	0.95	1300.00	0.96	0.96
0.14	0.96	0.96	14.00	0.97	0.96	1400.00	0.97	0.97
0.15	0.97	0.97	15.00	0.98	0.97	1500.00	0.98	0.98
0.16	0.98	0.98	16.00	0.98	0.97	1600.00	0.98	0.98
0.17	0.98	0.98	17.00	0.99	0.98	1700.00	0.99	0.98
0.18	0.99	0.99	18.00	0.99	0.99	1800.00	0.99	0.98
0.19	0.99	0.99	19.00	0.99	0.99	1900.00	0.99	0.99
0.20	0.99	0.99	20.00	0.99	0.99	2000.00	0.99	0.99
0.21	0.99	0.99	21.00	1.00	0.99	2500.00	1.00	0.99
0.22	1.00	1.00	22.00	1.00	1.00	2600.00	1.00	0.99
0.23	1.00	1.00	23.00	1.00	1.00	2700.00	1.00	1.00
0.24	1.00	1.00	24.00	1.00	1.00	2900.00	1.00	1.00

Table 7. Average concentration (mg/L) at the bottom of the crevice over time with water presence in the wall surface. Using a diffusion coefficient of 0.145 cm^2/s

Time (s)	Depth = 1 mm		Time (s)	Depth = 10 mm		Time (s)	Depth = 100 mm	
	dia. 1 mm	dia. 5 mm		dia. 1 mm	dia. 5 mm		dia. 1 mm	dia. 5 mm
0.00	0.00	0.00	0.00	0.00	0.00	0.00	0.00	0.00
0.01	0.13	0.14	1.00	0.13	0.13	100.00	0.11	0.11
0.02	0.38	0.39	2.00	0.38	0.38	200.00	0.30	0.30
0.03	0.57	0.58	3.00	0.56	0.56	300.00	0.41	0.42
0.04	0.70	0.71	4.00	0.70	0.70	400.00	0.48	0.49
0.05	0.79	0.80	5.00	0.79	0.79	500.00	0.52	0.52
0.06	0.86	0.86	6.00	0.85	0.85	600.00	0.54	0.55
0.07	0.90	0.90	7.00	0.89	0.90	800.00	0.55	0.56
0.08	0.93	0.93	8.00	0.93	0.93	900.00	0.56	0.57
0.09	0.95	0.96	9.00	0.95	0.95	1000.00	0.56	0.57
0.10	0.97	0.97	10.00	0.96	0.96	1100.00	0.57	0.57
0.11	0.98	0.98	11.00	0.97	0.97	1200.00	0.57	0.57
0.12	0.99	0.99	12.00	0.98	0.98	1300.00	0.57	0.57
0.13	0.99	0.99	13.00	0.98	0.98	1400.00	0.57	0.57
0.14	0.99	0.99	14.00	0.99	0.99	1500.00	0.57	0.57
0.15	1.00	1.00	15.00	0.99	0.99	2000.00	0.57	0.57
0.16	1.00	1.00	16.00	0.99	0.99	2500.00	0.57	0.57
0.17	1.00	1.00	17.00	0.99	0.99	5000.00	0.57	0.57
0.18	1.00	1.00	18.00	0.99	0.99	7000.00	0.57	0.57
0.19	1.00	1.00	19.00	0.99	0.99	9000.00	0.57	0.57
0.20	1.00	1.00	20.00	0.99	0.99	10000.00	0.57	0.57

Table 8. Average concentration (mg/L) at the bottom of the crevice over time with water presence in the wall surface. Using a diffusion coefficient of 0.097 cm^2/s

Time (s)	Depth = 1 mm		Time (s)	Depth = 10 mm		Time (s)	Depth = 100 mm	
	dia. 1 mm	dia. 5 mm		dia. 1 mm	dia. 5 mm		dia. 1 mm	dia. 5 mm
0.00	0.00	0.00	0.00	0.00	0.00	0.00	0.00	0.00
0.01	0.05	0.05	1.00	0.05	0.05	100.00	0.04	0.04
0.02	0.22	0.23	2.00	0.22	0.22	200.00	0.17	0.17
0.04	0.51	0.53	4.00	0.51	0.51	300.00	0.27	0.27
0.05	0.62	0.63	5.00	0.61	0.70	400.00	0.33	0.34
0.10	0.89	0.89	10.00	0.88	0.88	500.00	0.38	0.38
0.11	0.91	0.92	11.00	0.90	0.90	600.00	0.41	0.41
0.12	0.93	0.93	12.00	0.92	0.92	800.00	0.42	0.43
0.13	0.95	0.95	13.00	0.94	0.94	900.00	0.44	0.44
0.14	0.96	0.96	14.00	0.95	0.95	1000.00	0.44	0.45
0.15	0.97	0.97	15.00	0.96	0.96	1100.00	0.45	0.45
0.16	0.98	0.98	16.00	0.97	0.97	1200.00	0.45	0.46
0.17	0.98	0.98	17.00	0.97	0.97	1300.00	0.45	0.46
0.18	0.99	0.99	18.00	0.98	0.98	1400.00	0.45	0.46
0.19	0.99	0.99	19.00	0.98	0.98	1500.00	0.45	0.46
0.20	0.99	0.99	20.00	0.98	0.98	2000.00	0.45	0.46
0.21	0.99	0.99	21.00	0.98	0.98	2500.00	0.45	0.46
0.22	1.00	1.00	22.00	0.99	0.99	5000.00	0.45	0.46
0.23	1.00	1.00	23.00	0.99	0.99	7000.00	0.45	0.46
0.24	1.00	1.00	24.00	0.99	0.99	9000.00	0.45	0.46
0.25	1.00	1.00	25.00	1.00	1.00	10000.00	0.45	0.46

CHAPTER III
CHLORINE DIOXIDE GAS COMPATIBILITY OF PLASTICS AND ELASTOMERS TYPICALLY USED IN FOOD PROCESSING EQUIPMENT

This article hasn't been published anywhere, nor will it be before I turn in the final version of my ETD, so I didn't include a publication statement.

3.1. Abstract

Food safety is a concern for all individuals involved in the food supply chain. Besides controlling the food product itself to improve safety, washing and sanitizing surfaces and equipment are critical. Chlorine dioxide (ClO_2) is a green-yellow gas, known as a strong antimicrobial agent against multiple pathogenic microorganisms and effective on biofilms. Plastics such as polypropylene (PP), polyester (PET), cast nylon, ultra-high-molecular-weight polyethylene (UHMWPE), polytetrafluoroethylene (PTFE), polyvinylidene fluoride (PVDF) and white Acetal; and elastomers like nitrile rubber (NBR or Buna-N), ethylene propylene diene monomer (EPDM), and fluoroelastomer (FKM) are widely used in food processing surfaces and equipment. Although ClO_2 gas is a competent agent, the change in the physical properties of plastics and elastomers due to the exposure to the gas is a concern. The objective of this study was to determine the resistance to ClO_2 gas exposure for selected plastics and elastomers in terms of physical properties. Plastic (1.50 in X 0.50 in X 0.25 in) and elastomer samples (1.50 in X 0.50 in X 0.125 in) were exposed to 3000 ppm for 7 days inside a chamber following ASTM International Standards. After exposure, measurements of physical dimensions (thickness, length, and width), color, and hardness were made. Hardness was determined by a durometer (Shore A for elastomers and Shore D for plastics). Changes in values due to gas exposure were compared within the same material using ANOVA. After 7 days (168 hours) exposure at 3000 ppm of ClO_2 gas, none of the plastics or elastomers used showed a significant difference ($p<0.05$) in the hardness value. However, Acetal, Buna-N, EPDM, Nylon, PET, PTFE, PVDF, and UHMWPE each showed a significant change ($p<0.05$) in color (ΔE^*) due to the gas treatment (from 0.20 ± 0.21 to 9.52 ± 2.76, 0.25 ± 0.22 to 7.16 ± 1.56, 0.65 ± 0.73 to 2.54 ± 1.67, 0.25 ± 0.20 to 0.55 ± 0.21, 0.18 ± 0.16 to 9.74 ± 1.57, 0.37 ± 0.70 to 3.28 ± 0.68, 0.43 ± 0.68 to 1.88 ± 1.05, and 0.19 ± 0.12 to 1.59 ± 0.87, respectively). This study is a first attempt to generate data for consideration in the engineering design of food processing equipment sanitized using ClO_2 gas.

3.2. Introduction

Foodborne diseases result from the consumption of food contaminated with pathogenic bacteria, viruses, or parasites. The main sources of contamination are mostly unhygienic practices during food production, harvesting, preparation, and

equipment cleaning, and the lack of good agricultural practices (Adley & Ryan, 2016). In industrialized countries, around 30% of the population has experienced a foodborne illness. Food contamination may also occur due to cross-contamination from ingredients, the processing environment, including equipment or surfaces, or people involved in every stage of the process (Barach, et al., 2016; WHO, 2002).

Food safety is a concern for all individuals involved in the food supply chain. The management of food safety risks and food regulations are imperative to protect public health. One well-structured strategy to decrease foodborne disease is the implementation of a Food Safety Plan (Barach, et al., 2016). Once hazards are identified, preventive controls (sanitation, supply chain, process, and/or allergen controls) are established to prevent them. Sanitation controls are needed at the beginning of the food production operation. Without a clean facility, equipment and the environment can introduce potentially hazardous contamination (Barach, et al., 2016). To improve food safety, transfer of hazards from unsanitary objects or personnel to food, food packaging material, and food contact surfaces must be prevented. The most common method to decontaminate food products and surfaces is by the use of sanitizers. Any substance or mixture of substances that reduces - but does not completely destroy nor eliminate - the bacteria population on the equipment or environment in significant numbers are known as sanitizers. Sanitizers used in the food industry must be approved for use by EPA and regulated by FDA (Code of Federal Regulations Title 21. Part 178). (EPA, 1999; FDA, 2019b)

Chlorine dioxide (ClO_2), is an approved sanitizer allowed to be used as an aqueous solution on food-processing equipment and utensils at concentrations of at least 100 parts per million and not more than 200 parts per million available ClO_2 (FDA, 2019b). The interest in using gaseous ClO_2 as a sanitizer agent has been increasing in recent years. It is highly effective at short treatment times and relatively low concentrations. In food applications ClO_2 has been shown to be a strong antimicrobial agent against multiple pathogenic microorganisms such as *E. coli* O157:H7, *Listeria monocytogenes*, *Salmonella* spp., yeasts and molds that could be attached to the surface of food products and equipment (Netrami, 2011; Sun, Baldwin, & Bai, 2019; Sy, McWatters, & Beuchat, 2005; V. Trinetta, Morgan, & Linton, 2010).

Unfortunately, ClO_2 is a strong oxidizer and can be corrosive, so its repeated use on food equipment could ultimately result in damage or maintenance issues. A number of companies that manufacture food equipment have published compatibility charts for materials exposed to various chemicals. However, only a few include the resistance to ClO_2 and its precursors and these lists typically do not include the concentration of the chemical or the condition used during tests. To

date, the information available in these compatibility charts are vague and lack quantifiable data.
Several studies had been conducted to address the effectiveness of ClO_2 as an antimicrobial agent. Previous researchers have shown that a reduction >5 log CFU/cm^2 of *Listeria monocytogenes* on ready-to-eat meat processing equipment was achieved after a treatment of 2mg/L (~724 ppm) of ClO_2 gas for 30 min (Trinetta, Vaid, Xu, Linton, & Morgan, 2012). However, no studies could be found to address the effect of ClO_2 on the different types of material used in food equipment. Therefore, the main objective of this work was to determine the effect of ClO_2 gas exposure on the physical properties of plastics and elastomers used in food equipment. This test aimed to evaluate physical changes, specifically hardness and color properties, of seven plastics and three elastomers. A treatment of constant ClO_2 gas exposure at 3000 ppm for 7, 14, and 21 days was applied to the materials. These treatments were equivalent to a cumulative effect of 504000, 1008000, and 1512000 ppm·h, respectively of gas exposure. When considering typical treatment conditions for equipment sanitization mentioned above (724 ppm for 0.5 hours), the cumulative exposure is equivalent to ~1392, 2784, and 4176 applications of ClO_2 gas.

3.3. Materials and methods

Testing was based on three standard methods from the American Society for Testing and Material (ASTM International) and included: the standard practice for evaluating the resistance of plastics to chemical reagents [D543-14], the standard test method for rubber property – durometer hardness [D2240-15], and the standard practice for conditioning plastics for testing [D618-14]. These three standard methods were adapted to address the resistance of selected plastics and elastomers to ClO_2 gas exposure.

3.3.1. Schematic system - gas generation

The gas generation and treatment system (Figure 12) included a ClO_2 gas generator (Enerfab, Inc.; Cincinnati, OH), a 0.422 m^3 stainless steel tank (reservoir), a 2.883 $\times 10^{-3}$ m^3 stainless steel exposure chamber (treatment chamber), and a detection system that was able to control, monitor, and record ClO_2 gas concentration in real-time. The experiments were run at room temperature (23 ± 2˚C), 50% ± 10% relative humidity, following ASTM International Standards D618-14, and under dark conditions.

From a cylinder containing a mixture of [2%] chlorine (Cl_2) gas and [98%] nitrogen (N_2), gas was injected through a sodium chlorite [74%] cartridge to generate ClO_2 gas. The generated ClO_2 gas [4%] was introduced into the stainless steel reservoir tank. The gas was pumped from the reservoir into the stainless steel treatment chamber using a diaphragm pump. An outlet valve remained open to maintain pressure equilibrium inside the reservoir. The system was designed to achieve a target gas concentration of approximately 3000 ppm ± 100 ppm in the treatment chamber. A programmable logic controller (PLC) DL06 (Automation Direct, GA, USA) and human-machine interface EZ-S6M-R (EZAutomation, IA, USA) was used to control a solenoid valve that injected ClO_2 gas from the reservoir into the treatment chamber. To control the desired concentration, the gas was pumped to an Optek sensor, Model AF26 (OPTEK Technology, Inc., TX, USA) and back to the chamber. The PLC controller was able to inject gas automatically to keep the desired concentration.

The OPTEK sensor uses dual detectors to measure the transmission of light through the sensor at two wavelengths (385 and 550 nm) simultaneously. The measure of ClO_2 concentration is based on the relative absorption of these two wavelengths. This sensor was connected to an Optek Control 4000 photometric converter (OPTEK Technology, Inc., TX, USA), which converted the light absorption by the gas to concentration (ppm in the air) in real-time. During the experiment, gas concentration was recorded using a midi data logger GL240 (Graphtec America Inc., CA, USA) connected to the Optek Control 4000 to record voltage proportional to the signal from the sensor. This reading was directly related to the concentration of gas in the headspace of the treatment chamber.

For the purpose of this study, ClO_2 gas concentration was expressed as ppm in the air (~362 ppmv equals 1 mg/L in the air). The gas phase concentration was recorded based on the following calibration curve:

$$\mathbf{y = 1130.5\,x - 812.48} \qquad (\mathbf{3.3.1})$$

where, x is the voltage (V) record by the midi data logger, and y is the ClO_2 gas concentration in ppmv.

3.3.2. Material Samples

For this study, a total of 10 materials were exposed to the ClO_2 gas. Seven different plastics were selected: polypropylene (PP), polyethylene terephthalate (PET), cast nylon, ultra-high molecular weight polyethylene (UHMWPE), polytetrafluoroethylene (PTFE), polyvinylidene fluoride (PVFD), and acetal resin.

Three different elastomers were also selected: white nitrile butadiene (BUNA-N), ethylene propylene diene monomer (EPDM), and fluoroelastomer (FKM). The dimensions for the plastics were 38.10 x 12.70 mm (1.50 x 0.50 inches), and 6.35 mm (0.25 inches) thickness. For elastomers, the dimensions were 38.10 x 12.70 mm (1.50 x 0.50 inches), and 3.175 mm (0.125 inches) thickness.

3.2.3. Exposure Tests

Testing was based on the ASTM International Standard Practices for evaluating the resistance of plastics to chemical reagents D543-14. Modifications to this standard were done, where the mechanical properties resistance of plastics and elastomers was analyzed based on hardness value instead of the tensile properties test. Seven different plastic samples and three elastomer samples were prepared based on the standard methods ASTM International Standards D543-14, and D618-14. Three specimens for each type of material were prepared and treated at the target concentration of ClO_2 gas (3000 ± 100 ppm). Three control (no gas exposure) specimens for each type of material were also evaluated. In each of three replicates, three samples of each material were constantly exposed to 3000 ± 100 ppm of gas for 7 days in the treatment chamber. Before and after treatment, each specimen's initial weight, dimensions, hardness, and color were measured and recorded. Additionally, the samples from the first replicate were re-exposed to gas for an additional 7 and 14 days resulting in samples' exposed (and their properties measured) for 7, 14, and 21 days. This re-exposure was not replicated.

3.3.4. Hardness measurement

The hardness value determines the relative hardness of materials by correlating the depth of an indentation produced by a durometer with a known amount of compressive force, based on the ASTM International Standard ASTM D2240.15. Six specimens for each material were measured using the durometer (Type D for plastics and Type A for elastomers) before and after the ClO_2 gas treatment for each replicate. Three control and three treated specimens were measured for each material per replicate with three replicates.

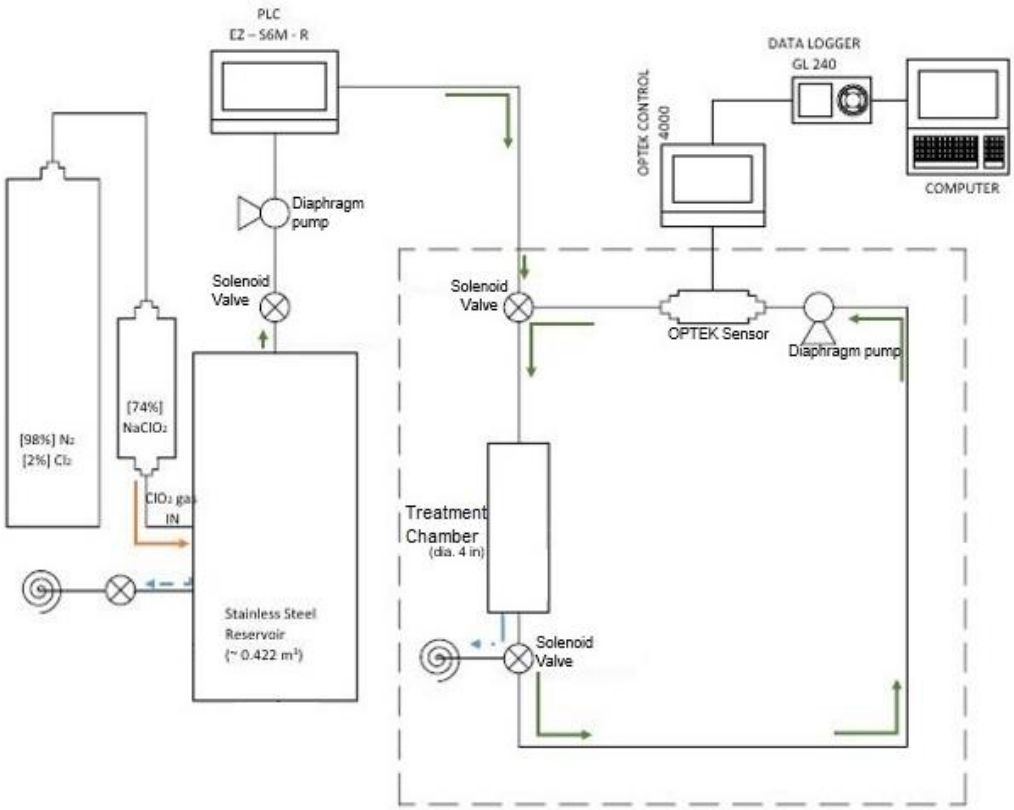

Figure 12. Schematic setup for evaluating material compatibility to constants ClO_2 gas exposure.

The surfaces of each specimen were flat and parallel over an area to permit the presser foot durometer to contact the specimen (Figure 13), while the specimen was supported to provide stability for the indentor point to assure a steady reading. Before measuring, each specimen was placed on a flat, hard, horizontal surface. Then, the durometer was held in a vertical position, with the indentor tip at a minimum distance of 6.0 mm (0.24 in.) from any edge. Finally, the presser foot was applied to each specimen and kept in a vertical position with a firm smooth downward action. Sufficient pressure was needed to assure firm contact between the presser foot and the specimen. Additionally, three rubber reference blocks for Shore A scale were used to provide verification of readings by the Durometer (Type A). One metal reference block provided a reading verification for the Durometer (Type D).

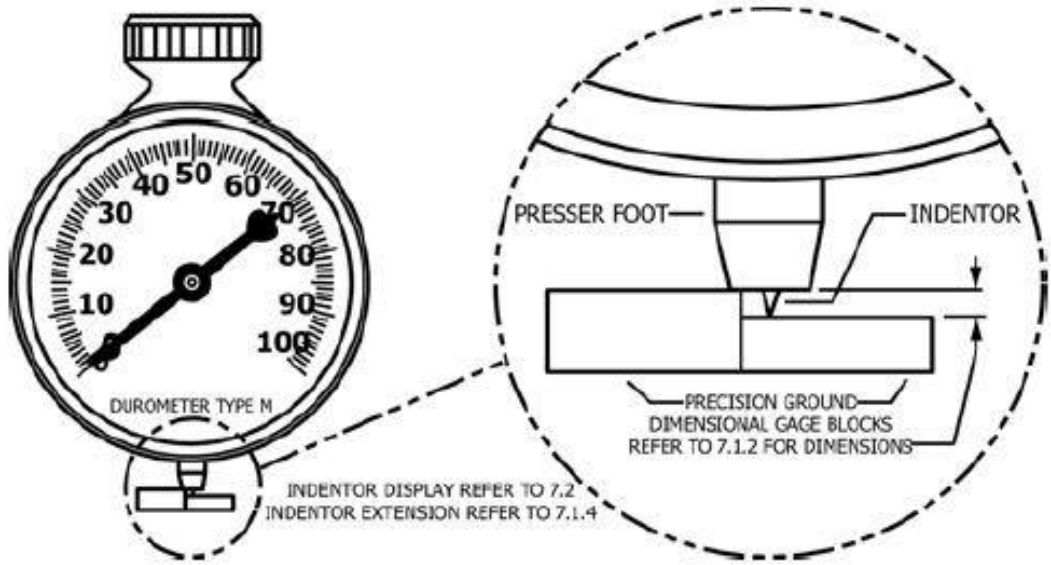

Figure 13. Schematic description of durometer equipment. Adapted from ASTM International Standard D2240-15

Durometers are scaled from 0 to 100, based on the amount of compressive force (Table 9). For each specimen, three readings of hardness at different positions on the specimen were determined, and the arithmetic mean was calculated. Once the mean is determined, the values were converted into force for better interpretation. Readings were recorded for each specimen for all materials for treated (triplicates) and control (triplicates) samples. Hardness measurement was measured as shore A or D value, and reported as its equivalent in Young's modulus, which is a mechanical property that measures the stiffness of a solid material, based on the relationship between stress and strain in the linear elasticity.

$$\log_{10}\mathrm{E} = 0.0235 \cdot \mathrm{S} - 0.6403 \tag{3.3.2}$$

$$S = S_A \tag{3.3.3}$$

$$S = S_D + 50 \tag{3.3.4}$$

The equation 3.3.2 is the Neo-Hookean linear relation between the ASTM D2240 hardness value and material elastic modulus, where E is the Young's modulus in MPa, S_A represents shore A hardness, and S_D represents shore D hardness.

Table 9. Durometer equipment amount of compressive force [N]

Indicated Value	Type A	Type D
0	0.55	0.000
10	1.30	4.445
20	2.05	8.890
30	2.80	13.335
40	3.55	17.780
50	4.30	22.225
60	5.05	26.670
70	5.80	31.115
80	6.55	35.560
90	7.30	40.005
100	8.05	44.450
N/ durometer unit	0.075	0.4445
Spring calibration tolerance	± 0.075 N	± 0.4445 N

3.3.5. Color measurement

The color of each material sample was measured using a Chroma Meter CM – 508d (Konica Minolta Holdings, Inc., NJ, USA). The meter was set on the L* a* b* scale, the observer was CIE 10° Standard Observer, and the illuminant selected was CIE Standard D65. Additionally, the Chroma meter was calibrated on a white tile. Six specimens for each material were measured before and after the ClO_2 gas treatment. Each specimen for all materials for treated (triplicates) and control (triplicates) samples were measured and expressed using the CIE-L* a* b* uniform color space (CIELAB, 1976). The total difference in color due to gas exposure was addressed by evaluating ΔE*, which is a positive value calculated based on the change in the L*, a*, and b* parameters using the equation below. The total difference was compared between treated and control samples of the same material.

$$\Delta E^* = \sqrt{(L_2^* - L_1^*)^2 + (a_2^* - a_1^*)^2 + (b_2^* - b_1^*)^2} \qquad (3.3.5)$$

3.3.6. Statistical analysis of data

The effects of time and treatment on hardness and color of each material were analyzed using one-way repeated ANOVA with treatment as the between-subject

effect and time as the within-subject effect. Diagnostic analysis was conducted to examine model assumptions for normality and equal variance. Post hoc multiple comparisons were performed with Tukey's adjustment. Statistical significance was identified at the level of 0.05. Analyses were conducted in SAS 9.4 TS1M4 for Windows 64x (SAS institute Inc., Cary, NC).

3.4. Results and discussion

All six specimens for each material were similar in dimensions. Table 10 lists the dimensions and weight for the selected plastics and elastomers. None of the materials showed a significant difference in dimensions and weight after treatment for 7, 14, and 21 days.

3.4.1. Hardness measurement

Table 11 list the mechanical properties of plastics materials exposed to 3000 ± 100 ppm of ClO_2 gas for 0 and 7 days. For the seven plastics: Acetal, Nylon, PET, PP, PTFE, PVDF, and UHMWPE, the initial Young Modulus (day 0) was 289.8, 214.3, 268.6, 182.7, 81.3, 225.24, and 104.1 MPa, respectively (Figure 14). Meanwhile, Table 12 shows the mechanical properties of three elastomers: Buna-N, EPDM, and FKM withinitial Young's Modulus of 7.1, 13.9, and 6.9 MPa, respectively (Figure 15). After materials were exposed for 7 days (168 hours) at 3000 ppm of ClO_2 gas, none of the plastics or elastomers showed a significant difference ($p<0.05$) in the hardness value (Figure 14, 15).

Table 10. Material dimensions

Material	Width (mm)	Length (mm)	Thickness (mm)	Weight (g)
Acetal	12.50 ± 0.21	37.66 ± 0.69	6.72 ± 0.05	4.479 ± 0.410
Nylon	13.00 ± 0.15	41.38 ± 0.10	7.00 ± 0.09	4.058 ± 0.042
PET	12.58 ± 0.53	38.02 ± 0.08	6.87 ± 0.09	4.340 ± 0.007
PP	13.12 ± 0.19	40.03 ± 0.13	6.39 ± 0.07	2.897 ± 0.046
PTFE	12.71 ± 0.07	37.71 ± 0.17	5.93 ± 0.68	6.216 ± 0.123
PVDF	12.15 ± 0.09	37.69 ± 0.22	7.32 ± 0.09	5.726 ± 0.025
UHMWPE	12.71 ± 0.10	37.55 ± 0.72	6.57 ± 0.08	2.846 ± 0.003
BUNA-N*	13.25 ± 0.20	37.99 ± 0.20	3.18 ± 0.03	2.435 ± 0.040
EPDM*	13.38 ± 0.65	38.31 ± 0.31	3.44 ± 0.05	3.431 ± 0.171
FKM*	13.28 ± 0.42	38.18 ± 0.70	3.01 ± 0.03	1.875 ± 0.068

Note: Values are reported as average ± S.D.
Note: * - Elastomers

3.4.1. Hardness measurement

Table 11 list the mechanical properties of plastics materials exposed to 3000 ± 100 ppm of ClO_2 gas for 0 and 7 days. For the seven plastics: Acetal, Nylon, PET, PP, PTFE, PVDF, and UHMWPE, the initial Young Modulus (day 0) was 289.8, 214.3, 268.6, 182.7, 81.3, 225.24, and 104.1 MPa, respectively (Figure 14). Meanwhile, Table 12 shows the mechanical properties of three elastomers: Buna-N, EPDM, and FKM withinitial Young's Modulus of 7.1, 13.9, and 6.9 MPa, respectively (Figure 15). After materials were exposed for 7 days (168 hours) at 3000 ppm of ClO_2 gas, none of the plastics or elastomers showed a significant difference ($p<0.05$) in the hardness value (Figure 14, 15).

To date, no studies have quantitatively shown the compatibility of materials to ClO_2 gas based on physical property experiments. However, some charts have been generated based on experience. These charts mention that plastics such as PVDF and PTFE are recommended to be used in surfaces (piping materials) and equipment (pump fitting) exposed to ClO_2 (Gates, 1998; GRACO, 2013). However, PP is also used as piping material (Gates, 1998) and reported as not recommended to be used with ClO_2 (GRACO, 2013). Additionally, FKM was determined to be sometimes acceptable, whilst EPDM is listed as poor compatibility (Gates, 1998; GRACO, 2013). Other charts showed that BUNA-N was not recommended to be used with ClO_2 because of its low compatibility to this chemical (GRACO, 2013). The information shown in Table 11 & Table 12 is a first step to develop data on compatibility for engineering design purposes.

3.4.2. Color measurement

The color properties for each material are listed Table 13. After 7 days of exposure to 3000 ppm of ClO_2 gas, the plastics Acetal, PET, PTFE, PVDF, and UHMWPE, showed a significant color difference (using equation 3.3.5) equal to: 9.52, 0.55, 9.74, 3.28, 1.88, and 1.59, respectively. Additionally, elastomers BUNA-N, EPDM, and FKM showed a significant color difference with 7.16, 2.54, and 2.28, respectively. Meanwhile, PP and Nylon (plastics) did not show a significant difference ($p<0.05$) in color. After 14 and 21 days of treatment, ΔE^* in the same materials that showed difference after 7 days tended to increase. Also, Table 13 shows PP and Nylon might change significantly in color after exposure for 21 days. The change in color could be a sign of reaction with the ClO_2. To date, no studies have quantified the effect of exposure to ClO_2 gas on color change in these materials.

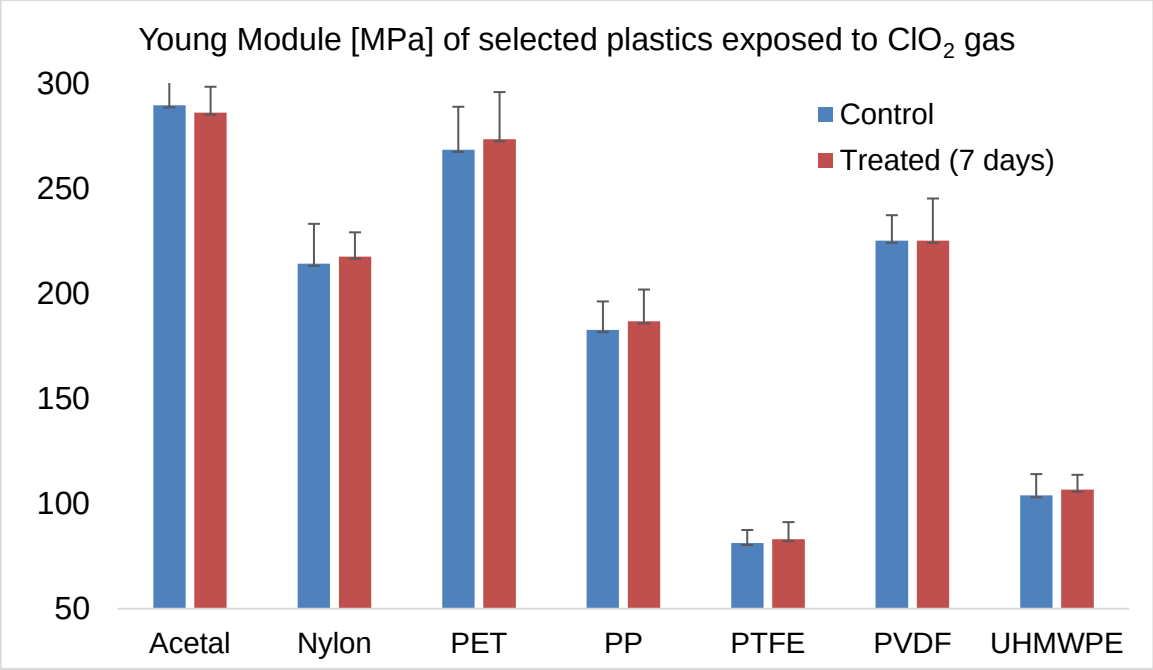

Figure 14. Plastics Young's module [MPa] value after ClO_2 gas exposure for 7 days at 3000 ppm.

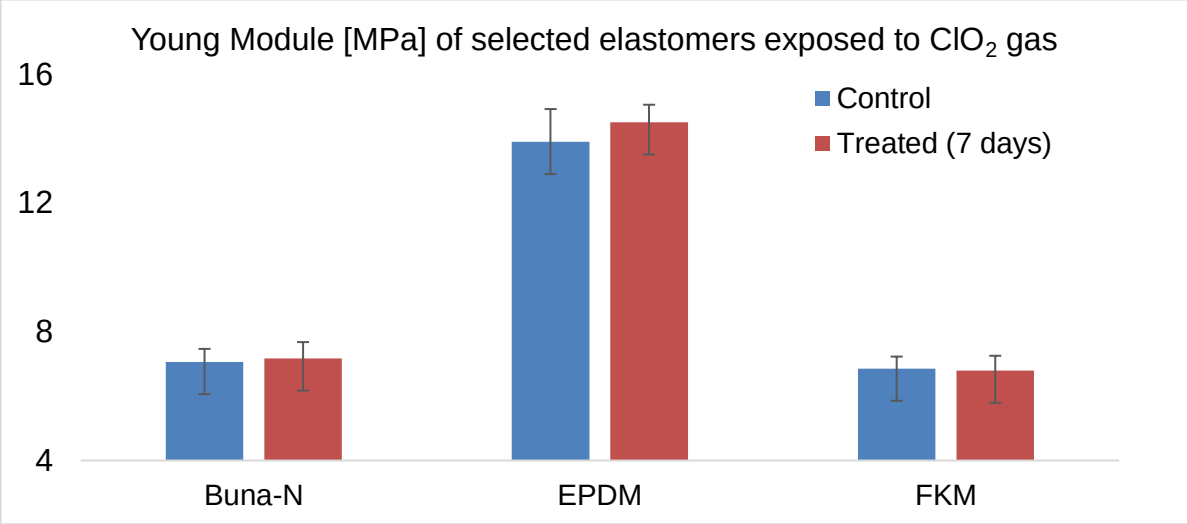

Figure 15. Elastomers hardness (N) value after and before ClO_2 gas exposure for 7 days at 3000 ppm

Table 11. Mechanical properties value for seven different plastics exposed to ClO2 gas (3000 ± 100 ppm) for 0, and 7 days

Material	ClO_2 gas (days)	Mechanical Properties		
		Shore D	Hardness (N)	Young Modulus (MPa)
Acetal	0	82.0 ± 0.78	36.4490 ± 0.3487	289.7873 ± 12.4302
	7	81.8 ± 0.80	36.3502 ± 0.3559	286.3304 ± 12.2771
Nylon	0	76.4 ± 1.64	33.9466 ± 0.7309	214.3157 ± 18.9933
	7	76.7 ± 0.99	34.0948 ± 0.4413	217.6892 ± 11.5896
PET	0	80.6 ± 1.50	35.8069 ± 0.6677	268.5831 ± 20.4849
	7	80.9 ± 1.65	35.9551 ± 0.7328	273.6282 ± 22.4403
PP	0	73.4 ± 1.37	32.6461 ± 0.6081	182.7238 ± 13.6300
	7	73.9 ± 1.46	32.8271 ± 0.6489	186.8724 ± 15.1606
PTFE	0	58.5 ± 1.48	25.9950 ± 0.6566	81.3389 ± 6.1500
	7	58.9 ± 1.99	26.1596 ± 0.8865	83.1734 ± 8.0779
PVDF	0	77.3 ± 1.00	34.3747 ± 0.4445	225.2400 ± 12.1855
	7	77.7 ± 1.69	34.5228 ± 0.7499	229.9108 ± 20.1321
UHMWPE	0	63.0 ± 1.90	28.0035 ± 0.8452	104.0685 ± 10.0481
	7	63.5 ± 1.22	28.2340 ± 0.5426	106.7324 ± 7.0415

Note: Values are represented as average ± S.D. (n=3)
Note: No significant difference ($p>0.05$) between the same plastics treated for 0 & 7 days.

Table 12. Mechanical properties value for three different elastomers exposed to ClO2 gas (3000 ± 100 ppm) for 0, and 7 days

Material	ClO_2 gas (days)	Mechanical Properties		
		Shore A	Hardness (N)	Young Modulus (MPa)
Buna-N	0	63.3 ± 1.07	4.7500 ± 0.0806	7.0589 ± 0.4095
	7	63.7 ± 1.39	4.7708 ± 0.1042	7.1729 ± 0.5062
EPDM	0	75.9 ± 1.43	5.6875 ± 0.1071	13.8991 ± 1.0192
	7	76.7 ± 0.69	5.7500 ± 0.0520	14.5098 ± 0.5428
FKM	0	62.6 ± 1.30	4.7097 ± 0.0780	6.8559 ± 0.3742
	7	62.8 ± 1.04	4.6958 ± 0.0978	6.7932 ± 0.4610

Note: Values are represented as average ± S.D. (n=3)
Note: No significant difference ($p<0.05$) between the same elastomers treated for 0 & 7 days.

Additional color differences were calculated based on the individual parameters L*, a*, and b*. For the selected material treated with 3000 ppm of ClO_2 gas for 7 days, Acetal (plastic) and EPDM (elastomer) showed a significant decrease for L* parameter from 78.06 to 77.69 and from 33.90 to 32.68, respectively (Table 13). The remaining plastics and elastomers did not show a significance change in L*. Table 13 shows that after 21 days, Nylon might decrease significantly, while Acetal and EPDM tended to keep decreasing. The decrease for these parameters implies the material was getting darker due to gas exposure over time.

Moreover, five plastics Acetal, PET, PTFE, PVDF, and UHMWPE treated with the gas for 7 days showed a significant difference for a* values, from -0.56 to -4.93, -0.97 to -4.80, -0.70 to -2.05, -1.60 to -2.30, respectively. This decrease in a* indicates ain increasingly greenish color in the plastics samples. Meanwhile, plastics Nylon and PP did not show a significant difference in the a* index value. Additionally, the elastomers white BUNA-N and EPDM showed a significant difference after being treated with the gas for 7 days, where the values of a* changed from 0.77 to -0.18 and 1.30 to 1.67. FKM did not show a significant difference in the a* index value. The decrement at the a* parameter implied the white materials were getting greener due to gas exposure over time, whilst the black elastomer (EPDM) was getting redder, even though the change imperceptible to the naked eyes. Table 13 shows that Nylon might increase significantly after 14 and 21 days of treatment.

After 7 days exposure to 3000 ppm of ClO_2 gas, plastics Acetal, PET, PTFE, PVDF, and UHMWPE showed a significant increment in the b* value, from -2.40 to 6.41, 1.93 to 11.76, -2.52 to 0.19, -4.48 to -3.07, and -12.09 to -10.75, respectively. Meanwhile, Nylon, and PP did not show significant changes (Table 13). After the treatment, the white BUNA-N elastomer showed a significant increment in the b* from -8.47 to 15.41. However, EPDM and FKM did not show a significant change. The increment in b* index implies a change in color from white to a yellowish color due to the 3000 ppm of ClO_2 gas. Table 13 shows that after Nylon might increase significantly after 21 days.

The change in color from the plastics such as Acetal, PET, PTFE, PVDF, and UHMWPE, and the white elastomer BUNA-N to a greenish and yellowish color, determined by the decrement in the a* and the increment in the b* value (CIELAB, 1976), agreed with the color of the gas, which is characterized to be a green-yellow gas (Gates, 1998) at low concentrations. Furthermore, FKM did not show a change in color to a green or yellow spectrum. This might be because the sample was black.

Table 13. Color properties of selected plastics and elastomers exposed for 0, 7, 14, and days to ClO_2 gas (3000 ppm) Material exposed for 14 and 21 days was not replicated

Material	Exposure to ClO_2 gas (days)	Color Properties			
		L*	a*	b*	ΔE*
Acetal	0	78.06 ± 0.23 (a)	- 0.56 ± 0.03 (a)	- 2.40 ± 0.30 (b)	-
	7	77.69 ± 0.31 (b)	- 4.93 ± 0.36 (b)	4.97 ± 0.30 (a)	9.52 ± 2.76 (-)
	14	77.39 ± 0.05 (*)	- 5.94 ± 0.08 (*)	11.54 ± 0.23 (*)	15.33 ± 0.30 (*)
	21	77.33 ± 0.37 (*)	- 5.69 ± 0.20 (*)	11.83 ± 0.16 (*)	15.52 ± 0.20 (*)
Nylon	0	71.06 ± 0.98	- 4.44 ± 0.11	- 4.86 ± 0.15	-
	7	71.06 ± 0.95	- 4.57 ± 0.23	- 4.85 ± 0.24	0.55 ± 0.21
	14	69.92 ± 1.04	- 4.30 ± 1.07	- 4.57 ± 0.17	2.28 ± 1.10
	21	68.52 ± 2.13 (*)	- 4.23 ± 2.23	- 3.60 ± 0.37 (*)	3.85 ± 2.30 (*)
PET	0	88.57 ± 0.59	- 0.97 ± 0.11 (a)	1.93 ± 0.17 (b)	-
	7	88.88 ± 0.22	- 4.80 ± 0.66 (b)	11.76 ± 0.33 (a)	9.74 ± 1.57 (-)
	14	87.45 ± 0.44	- 5.44 ± 0.18 (*)	13.76 ± 0.19 (*)	12.74 ± 0.34 (*)
	21	87.02 ± 0.37	- 5.37 ± 0.37 (*)	14.39 ± 0.39 (*)	13.34 ± 0.70 (*)
PP	0	38.93 ± 0.66	0.36 ± 0.22	- 3.69 ± 0.47	-
	7	39.44 ± 0.56	0.46 ± 0.30	- 4.28 ± 0.66	1.02 ± 0.70
	14	39.39 ± 0.83	0.51 ± 0.13	- 4.01 ± 0.50	0.83 ± 0.06
	21	39.15 ± 0.86	0.31 ± 0.23	- 3.73 ± 0.44	0.69 ± 0.45 (*)
PTFE	0	90.83 ± 1.26	- 0.70 ± 0.14 (a)	- 2.52 ± 0.43 (b)	-
	7	91.01 ± 0.68	- 2.05 ± 0.33 (b)	0.19 ± 0.54 (a)	3.28 ± 0.68 (-)
	14	90.88 ± 0.71	- 2.28 ± 0.07 (*)	0.88 ± 0.61 (*)	4.29 ± 0.42 (*)
	21	90.31 ± 0.91	- 2.36 ± 0.03 (*)	1.36 ± 0.23 (*)	4.74 ± 0.02 (*)

Note: a-b. Different letters indicate significant difference among data in the column within the same material at 0 and 7 days ($p < 0.05$)
Note: (-) Indicate significant difference among data in the column within the same material between 0 and 7 days ($p < 0.05$)
Note: (*) Indicate significant difference among data in the column within the same material between 0, 14, and 21 days ($p < 0.05$)

Table 13. Continued

Material	Exposure to ClO_2 gas (days)	Color Properties			
		L*	a*	b*	ΔE*
PVDF	0	60.66 ± 0.43	- 1.60 ± 0.20 (a)	- 4.48 ± 0.51 (b)	-
	7	60.86 ± 0.27	- 2.30 ± 0.35 (b)	- 3.07 ± 0.55 (a)	1.88 ± 1.05 (-)
	14	60.08 ± 0.21	- 2.52 ± 0.12 (*)	- 2.59 ± 0.16 (*)	2.53 ± 0.28 (*)
	21	60.01 ± 0.34	- 2.79 ± 0.04 (*)	- 1.86 ± 0.22 (*)	3.30 ± 0.45 (*)
UHMWPE	0	58.81 ± 0.65	- 1.19 ± 0.06 (a)	- 12.09 ± 0.18 (b)	-
	7	58.75 ± 0.48	- 1.85 ± 0.47 (b)	- 10.75 ± 0.69 (a)	1.59 ± 0.87 (-)
	14	57.79 ± 0.76	- 1.90 ± 0.10 (*)	- 10.53 ± 0.04 (*)	1.93 ± 0.15 (*)
	21	58.19 ± 0.19	- 1.77 ± 0.03 (*)	- 10.83 ± 0.16 (*)	1.65 ± 0.18 (*)
Buna-N	0	83.18 ± 0.85	0.77 ± 0.17 (a)	8.47 ± 0.77 (b)	-
	7	82.94 ± 1.12	- 0.18 ± 0.50 (b)	16.19 ± 1.13 (a)	7.16 ± 1.56 (-)
	14	82.32 ± 0.56	0.40 ± 0.20 (*)	16.00 ± 0.48 (*)	8.45 ± 0.08 (*)
	21	82.62 ± 0.91	0.07 ± 0.23 (*)	15.16 ± 0.37 (*)	7.59 ± 0.10 (*)
EPDM	0	33.90 ± 1.39 (a)	1.30 ± 0.32 (b)	- 3.69 ± 0.61	-
	7	32.68 ± 0.43 (b)	1.67 ± 0.35 (a)	- 4.35 ± 0.84	2.54 ± 1.67 (-)
	14	32.20 ± 0.33 (*)	1.90 ± 0.04 (*)	- 4.60 ± 0.19 (*)	3.36 ± 0.95 (*)
	21	31.79 ± 0.15 (*)	1.82 ± 0.14 (*)	- 4.25 ± 0.31 (*)	3.63 ± 1.22 (*)
FKM	0	28.55 ± 0.51	1.61 ± 0.23	- 4.13 ± 0.67	-
	7	28.05 ± 0.54	1.98 ± 0.46	- 5.03 ± 0.99	2.28 ± 2.60 (-)
	14	28.01 ± 0.16	2.40 ± 0.24 (*)	- 5.43 ± 0.23 (*)	1.84 ± 0.31 (*)
	21	27.88 ± 0.24	2.09 ± 0.21 (*)	- 5.04 ± 0.47 (*)	1.41 ± 0.74 (*)

Note: a-b. Different letters indicate significant difference among data in the column within the same material at 0 and 7 days ($p < 0.05$)
Note: (-) Indicate significant difference among data in the column within the same material between 0 and 7 days ($p < 0.05$)
Note: (*) Indicate significant difference among data in the column within the same material between 0, 14, and 21 days ($p < 0.05$)
Note: + Elastomers

3.5. Conclusions

The goal of this chapter was to determine the chemical resistance of ten materials typically used in the food industries in equipment to ClO_2 gas exposure. The resistance was evaluated at constant exposure to 3000 ± 100 ppm for 7 days of the gas. This research aimed to provide information that could be generated for engineering design purposes, which is recently unavailable.

After 7 days, none of the materials (Acetal, Nylon, PET, PP, PTFE, PVDF, UHMWPE, BUNA-N, EPDM, and FKM) showed a significant impact in the mechanical properties due to the ClO_2 gas exposure. This data suggests that the gas treatment did not affect any of these materials after 168 hours of 3000 ppm. Despite no detectable changes in the hardness value for the materials, five plastics (Acetal, PET, PTFE, PVDF, and UHMWPE) and three elastomers (Buna-N, EPDM, and FKM) showed a change in overall color. This change in color could be used as a sign of interaction of the materials with the ClO_2 gas. Additional research is needed to generate data useful for future reference for engineering design.

To expand the research, longer exposure treatments are needed to address any possible hardness change due to the ClO_2 gas. Further research can also be extended to determining the impact of constant gas treatment against repeated, shorter-duration treatment cycles that are used in sanitation operations.

LIST OF REFERENCES

A. Schaub, S., T. Hargett, H., Kamrud, K., R. Sterling, C., & Marshall, M. (1993). Evaluation of Chlorine Dioxide Generated In-Situ for Disinfection of Waterborne Micro-Organisms. 34.

Abraham, A., Al-Khaldi, S., Assimon, S. A., Beaudry, C., Benner, R. A., Bennett, R., Binet, R., Cahill, S. M., Burkhardt, W., Chen, Y., Day, J., Deeds, J., DeGrasse, S., DePaola, A., Feng, P., Foley, S., Fry, F. S., Granade, H. R., Hait, J., Hammack, T., Hartman, G., Jones, J. L., Kase, J., Lampel, K. A., Myerts, M. J., Nayak, R., Nsofor, O., Orlandi, P. A., Pawar, R. S., Schlesser, J., Sharma, S., Stewart, D., Tallents, S. M., Trucksess, M. W., Zhang, G., & Ziobro, G. (2012). *Bad Bug Book: Foodborne Pathogenic Microorganisms and Natural Toxins Handbook* (Second Edition ed.): Center for Food Safety and Applied Nutrition. Food and Drug Administration (FDA). U.S. Department of Health and Human Services.

Adley, C. C., & Ryan, M. P. (2016). Chapter 1 - The Nature and Extent of Foodborne Disease. In J. Barros-Velázquez (Ed.), *Antimicrobial Food Packaging*, (pp. 1-10). San Diego: Academic Press.

Aieta, E. M., & Berg, J. D. (1986). A Review of Chlorine Dioxide in Drinking Water Treatment. *78*(6), 62-72.

Allata, S., Valero, A., & Benhadja, L. (2017). Implementation of traceability and food safety systems (HACCP) under the ISO 22000:2005 standard in North Africa: The case study of an ice cream company in Algeria. *Food Control, 79*, 239-253.

Arango, J., Rubino, M. I., Auras, R., Rachford, A. A., Bai, Z. F., Grzesiak, A. L., & Kijchavengkul, T. (2014). In situ quantification of chlorine dioxide gas consumption by fresh produce using UV-visible spectroscopy. *Journal of Food Engineering, 131*, 75-81.

Barach, J., Fraser Heaps, J., Deibel, K., Mazzotta, A., Jackson, T., Scimeca, J., Estes, S., Allan, J., Shebuski, J., Mavity, S., & Feldstein, F. (2016). *Preventive Controls for Human Food* (First Edition ed.): Food Safety Preventive Controls Alliance (FSPCA). Food and Drug Administration (FDA). Illinois Institute of Technology's Institute for Food Safety and Health (IFSH).

Beresford, M. R., Andrew, P. W., & Shama, G. (2001). Listeria monocytogenes adheres to many materials found in food-processing environments. *Journal of Applied Microbiology, 90*(6), 1000-1005.

Bird, R. B., Stewart, W. E., & Lightfoot, E. N. (2006). Diffusivity and the Mechanisms of Mass Transport. In L. Wiley (Ed.), *Transport Phenomena, Revised 2nd Edition* Second ed., vol. 2nd Edition). University of Wisconsin-Madison.

Bridier, A., Briandet, R., Thomas, V., & Dubois-Brissonnet, F. (2011). Resistance of bacterial biofilms to disinfectants: a review. *Biofouling, 27*(9), 1017-1032.

Bridier, A., Sanchez-Vizuete, P., Guilbaud, M., Piard, J. C., Naitali, M., & Briandet, R. (2015). Biofilm-associated persistence of food-borne pathogens. *Food Microbiology, 45*, 167-178.

CDC. (2019). E. coli and Food Safety. In Secondary CDC (Ed.), *Secondary E. coli and Food Safety*, vol. Volume (pp. Pages): Centers for Disease Control and Prevention; National Center for Emerging and Zoonotic Infectious Diseases.Retrieved from https://www.cdc.gov/Features/ecoliinfection/.Accessed August 15, 2019

Chai, H.-E., Hwang, C.-A., Huang, L., Wu, V. C. H., & Sheen, L.-Y. (2020). Feasibility and efficacy of using gaseous chlorine dioxide generated by sodium chlorite-acid reaction for decontamination of foodborne pathogens on produce. *Food Control, 108*, 106839.

CIELAB. (1976). CIELAB Colour System. In). Paris, France: Commission International de Eclairage.

Dalton, C. B., Austin, C. C., Sobel, J., Hayes, P. S., Bibb, W. F., Graves, L. M., Swaminathan, B., Proctor, M. E., & Griffin, P. M. (1997). An Outbreak of Gastroenteritis and Fever Due to Listeria monocytogenes in Milk. *336*(2), 100-106.

Davey, M. E., & O'Toole, G. A. (2000). Microbial biofilms: from ecology to molecular genetics. *Microbiology and Molecular Biology Reviews, 64*(4), 847.

Davis, H. F., & Lee, Y. T. (1996). Photodissociation dynamics of OClO. *105*(18), 8142-8163.

Dourou, D., Beauchamp, C. S., Yoon, Y., Geornaras, I., Belk, K. E., Smith, G. C., Nychas, G.-J. E., & Sofos, J. N. (2011). Attachment and biofilm formation by Escherichia coli O157:H7 at different temperatures, on various food-contact surfaces encountered in beef processing. *International Journal of Food Microbiology, 149*(3), 262-268.

EPA. (1999). Selected EPA-Registered Disinfectants. In Secondary EPA (Ed.), *Secondary Selected EPA-Registered Disinfectants*, vol. Volume (pp. Pages): United States Environmental Protection Agency (EPA).Retrieved fromhttps://www.epa.gov/pesticide-registration/selected-epa-registered-disinfectants.Accessed

FDA. (2019a). PART 173 -- SECONDARY DIRECT FOOD ADDITIVES PERMITTED IN FOOD FOR HUMAN CONSUMPTION. In F. a. D. A. (FDA) (Ed.), *TITLE 21--FOOD AND DRUGS*, vol. 21CFR173.300): Food and Drugs Administration (FDA)

FDA. (2019b). PART 178 -- INDIRECT FOOD ADDITIVES: ADJUVANTS, PRODUCTION AIDS, AND SANITIZERS. In F. a. D. A. (FDA) (Ed.), *TITLE*

21--FOOD AND DRUGS, vol. 21CFR178.1010): Food and Drugs Administration (FDA).
Fu, Y., Zhang, K., Wang, N., & Du, J. (2007). Effects of aqueous chlorine dioxide treatment on polyphenol oxidases from Golden Delicious apple. *LWT - Food Science and Technology, 40*(8), 1362-1368.
Ganiev, I., Timergazin, Q., Kabalnova, N., Shereshovets, V., & Tolstikov, G. J. E. C.-T. J. (2005). Reactions of chlorine dioxide with organic compounds. *7*(1), 1-31.
Gates, D. J. (1998). Properties and Chemistry of Chlorine Dioxide. In W. D. Series (Ed.), *The Chlorine Dioxide Handbook*). United States of America: American Water Works Association.
Gómez-López, V. M., Ragaert, P., Jeyachchandran, V., Debevere, J., & Devlieghere, F. (2008). Shelf-life of minimally processed lettuce and cabbage treated with gaseous chlorine dioxide and cysteine. *International Journal of Food Microbiology, 121*(1), 74-83.
GRACO. (2013). Chemical Compatibility Guide. In).
Hosni, A. A., Jang, A., Coughlin, M., & Bishop, P. L. (2006). Diffusion of chlorine dioxide through aqueous and oil films. *Food and Bioproducts Processing, 84*(C4), 346-352.
Kaczur, J., & W. Cawlfield, D. (2000). Chlorine Oxygen Acids and Salts, Chlorous Acid, Chlorites, and Chlorine Dioxide. In).
Kadariya, J., Smith, T. C., & Thapaliya, D. (2014). Staphylococcus aureus and staphylococcal food-borne disease: an ongoing challenge in public health. *BioMed research international, 2014*, 827965-827965.
Kafetzopoulos, D. P., Psomas, E. L., & Kafetzopoulos, P. D. (2013). Measuring the effectiveness of the HACCP Food Safety Management System. *Food Control, 33*(2), 505-513.
Lee, Burgess, G., Rubino, M., & Auras, R. (2015). Reaction and diffusion of chlorine dioxide gas under dark and light conditions at different temperatures. *Journal of Food Engineering, 144*, 20-28.
Mueller, H. S. P., & Willner, H. (1993). Vibrational and electronic spectra of chlorine dioxide, OClO, and chlorine superoxide ClOO, isolated in cryogenic matrixes. *The Journal of Physical Chemistry, 97*(41), 10589-10598.
Netrami, S. (2011). *Utilization of chlorine dioxide gas in food packaging application.* Unpublished Dissertation, Michigan State University.
Olanya, O. M., Annous, B. A., & Taylor, J. (2015). Effects of Pseudomonas chlororaphis and gaseous chlorine dioxide on the survival of Salmonella enterica on tomatoes. *International Journal of Food Science and Technology, 50*(5), 1102-1108.
Pan, T., & Zhu, B. (1998). Study on diffusion–reaction process inside a cylindrical catalyst pellet. *Chemical Engineering Science, 53*(5), 933-946.

Park, S.-H., & Kang, D.-H. (2015). Antimicrobial effect of chlorine dioxide gas against foodborne pathogens under differing conditions of relative humidity. *LWT - Food Science and Technology, 60*(1), 186-191.

Pozo, V. F., & Schroeder, T. C. (2016). Evaluating the costs of meat and poultry recalls to food firms using stock returns. *Food Policy, 59*, 66-77.

Saengnil, K., Chumyam, A., Faiyue, B., & Uthaibutra, J. (2014). Use of chlorine dioxide fumigation to alleviate enzymatic browning of harvested 'Daw' longan pericarp during storage under ambient conditions. *Postharvest Biology and Technology, 91*, 49-56.

Sander, R. (2015). Compilation of Henry's law constants (version 4.0) for water as solvent. *Atmos. Chem. Phys., 15*(8), 4399-4981.

Scallan, E., Hoekstra, R. M., Angulo, F. J., Tauxe, R. V., Widdowson, M.-A., Roy, S. L., Jones, J. L., & Griffin, P. M. (2011). Foodborne illness acquired in the United States--major pathogens. *Emerging infectious diseases, 17*(1), 7-15.

Scharff, R. L. (2012). Economic Burden from Health Losses Due to Foodborne Illness in the United States. *75*(1), 123-131.

Schlisselberg, D. B., & Yaron, S. (2013). The effects of stainless steel finish on Salmonella Typhimurium attachment, biofilm formation and sensitivity to chlorine. *Food Microbiology, 35*(1), 65-72.

Shynkaryk, M. V., Pyatkovskyy, T., Mohamed, H. M., Yousef, A. E., & Sudhir, K. S. (2015). Physics of fresh produce safety: role of diffusion and tissue reaction in sanitization of leafy green vegetables with liquid and gaseous ozone-based sanitizers. *Journal of Food Protection, 78*(12), 2108-2116.

Singh, N., Singh, R. K., Bhunia, A. K., & Stroshine, R. L. (2002). Efficacy of Chlorine Dioxide, Ozone, and Thyme Essential Oil or a Sequential Washing in Killing Escherichia coli O157:H7 on Lettuce and Baby Carrots. *LWT - Food Science and Technology, 35*(8), 720-729.

Sun, X. X., Baldwin, E., & Bai, J. H. (2019). Applications of gaseous chlorine dioxide on postharvest handling and storage of fruits and vegetables - A review. *Food Control, 95*, 18-26.

Sy, K. V., McWatters, K. H., & Beuchat, L. R. (2005). Efficacy of gaseous chlorine dioxide as a sanitizer for killing Salmonella, yeasts, and molds on blueberries, strawberries, and raspberries. *Journal of Food Protection, 68*(6), 1165-1175.

Tarr, P. I. (1995). Escherichia coli O157:H7: Clinical, Diagnostic, and Epidemiological Aspects of Human Infection. *Clinical Infectious Diseases, 20*(1), 1-8.

Taube, H., & Dodgen, H. (1949). Applications of Radioactive Chlorine to the Study of the Mechanisms of Reactions Involving Changes in the Oxidation State of Chlorine. *Journal of the American Chemical Society, 71*(10), 3330-3336.

Taylor, J., Wohlers, D., & Amata, R. (2004). Toxicological profile for chlorine dioxide and chlorite.

Taylor, M., Klaiber, H. A., & Kuchler, F. (2016). Changes in U.S. consumer response to food safety recalls in the shadow of a BSE scare. *Food Policy, 62*, 56-64.

Trinetta, Vaid, R., Xu, Q., Linton, R., & Morgan, M. (2012). Inactivation of Listeria monocytogenes on ready-to-eat food processing equipment by chlorine dioxide gas. *Food Control, 26*(2), 357-362.

Trinetta, V., Morgan, M. T., & Linton, R. H. (2010). Use of high-concentration-short-time chlorine dioxide gas treatments for the inactivation of Salmonella enterica spp. inoculated onto Roma tomatoes. *Food Microbiology, 27*(8), 1009-1015.

Tuladhar, E., Hazeleger, W. C., Koopmans, M., Zwietering, M. H., Beumer, R. R., & Duizer, E. (2012). Residual Viral and Bacterial Contamination of Surfaces after Cleaning and Disinfection. *78*(21), 7769-7775.

Vaida, V., & Simon, J. D. (1995). The photoreactivity of chlorine dioxide. *Science, 268*(5216), 1443-1448.

Walker, J. R. L., & Ferrar, P. H. (1998). Diphenol Oxidases, Enzyme-catalysed Browning and Plant Disease Resistance. *Biotechnology and Genetic Engineering Reviews, 15*(1), 457-498.

WHO. (1999). Chemistry of desinfectants and desinfectant by-product. In Secondary WHO (Ed.), *Secondary Chemistry of desinfectants and desinfectant by-product*, vol. Volume (pp. Pages): World Health Organization (WHO). Internation Programme on Chemical Safety (IPCS).Retrieved from https://www.who.int/ipcs/publications/ehc/216_disinfectants_part_2.pdf.Accessed

WHO. (2002). Food safety and foodborne illness. *biochimica clinica, 26*(4), 39.

Wolfram, T. (2017). Most Common Foodborne Pathogens. In Secondary Wolfram, T. (Ed.), *Secondary Most Common Foodborne Pathogens*, vol. Volume (pp. Pages).Retrieved from https://www.eatright.org/home foodsafety/safety-tips/food-poisoning/most-common-foodborne-pathogens.Accessed

Zare, S., Zheng, Y., & Buck, S. (2017). Examining the Effect of Food Recalls on Demand: The Case of Ground Beef in the U.S. *Southern Agricultural Economics Association*(2017 Annual Meeting, February 4-7, 2017, Mobile, Alabama).

VITA

Mario Ernesto Bermudez Gonzalez was born in Managua, Nicaragua on June 16, 1994. He graduated from Zamorano University, Honduras and received his Bachelor's degree in Food Science and Technology. He earned his Master of Science degree in Food Science from the University of Tennessee, Knoxville.